Supplement of "HR3DHG version 1: modelling the spatio-temporal dynamics of mercury in the Augusta Bay (southern Italy)"

Giovanni Denaro[1], Daniela Salvagio Manta[2], Alessandro Borri[3], Maria Bonsignore[2], Davide Valenti[1,4], Enza Quinci[2], Andrea Cucco[5], Bernardo Spagnolo[4,6,7], Mario Sprovieri[2], and Andrea De Gaetano[3]

[1]CNR-IRIB, Consiglio Nazionale delle Ricerche Istituto per la Ricerca e l'Innovazione Biomedica, Via Ugo La Malfa 153, I-90146 Palermo, Italy
[2]CNR-IAS, Consiglio Nazionale delle Ricerche Istituto per lo studio degli impatti Antropici e Sostenibilità in ambiente marino, U.O.S di Capo Granitola, Via del Faro 3, I-91020 Campobello di Mazara (TP), Italy
[3]CNR-IASI Biomathematics Laboratory, Consiglio Nazionale delle Ricerche Istituto di Analisi dei Sistemi ed Informatica "A. Ruberti", Via dei Taurini 19, I-00185 Rome, Italy
[4]Dipartimento di Fisica e Chimica "Emilio Segrè", Università di Palermo, Group of Interdisciplinary Theoretical Physics and CNISM, Unità di Palermo, Viale delle Scienze, Ed. 18, I-90128 Palermo, Italy
[5]CNR-IAS, Consiglio Nazionale delle Ricerche Istituto per lo studio degli impatti Antropici e Sostenibilità in ambiente marino, U.O.S. di Oristano, località Sa Mardini, I-09072 Torregrande (OR), Italy
[6]Radiophysics Department, National Research Lobachevsky State University of Nizhni Novgorod, 23 Gagarin Avenue, Nizhni Novgorod 603950, Russia
[7]Istituto Nazionale di Fisica Nucleare, Sezione di Catania, Via S. Sofia 64, I-90123 Catania, Italy

Correspondence: Alessandro Borri (alessandro.borri@iasi.cnr.it)

S1 The Advection-Diffusion-Reaction Model - Seawater Compartment

S1.1 Dissolved elemental mercury concentration

The spatio-temporal dynamics of the dissolved elemental mercury concentration (Hg^0) in the Augusta basin (Zhang et al., 2014; Melaku Canu et al., 2015; Whalin et al., 2007; Monperrus et al., 2007b; Bagnato et al., 2013) is described by the following partial differential equation (PDE):

$$\begin{aligned}\frac{\partial Hg^0}{\partial t} = & +\frac{\partial}{\partial x}\left[D_x\frac{\partial Hg^0}{\partial x}\right]-\frac{\partial}{\partial x}(v_x Hg^0)+\frac{\partial}{\partial y}\left[D_y\frac{\partial Hg^0}{\partial y}\right]-\frac{\partial}{\partial y}(v_y Hg^0)\\ & +\frac{\partial}{\partial z}\left[D_z\frac{\partial Hg^0}{\partial z}\right]-\frac{\partial}{\partial z}(v_z Hg^0)+k_{Ph-de}\cdot MeHg\\ & -(k_1+k_3)\cdot Hg^0+(k_2+k_4)\cdot Hg^{II}+S_L^0,\end{aligned} \tag{S1}$$

where

- v_x, v_y and v_z are the components of the velocity field $[m/h]$;
- D_x and D_y are the horizontal turbulent diffusivities $[m^2/h]$;
- D_z is the vertical turbulent diffusivity $[m^2/h]$;
- k_{Ph-de} is the rate constant for the photo-demethylation of methyl-mercury $[1/h]$;
- k_1 is the rate constant for the photo-oxidation of elemental mercury $[1/h]$;
- k_2 is the rate constant for the photo-reduction of inorganic mercury $[1/h]$;
- k_3 is the rate constant for the biological oxidation of elemental mercury $[1/h]$;
- k_4 is the rate constant for the biological reduction of inorganic mercury $[1/h]$;
- S_L^0 is the direct loads of elemental mercury $[ng\cdot l^{-1}\cdot h^{-1}]$.

The integration domain of the PDE is constituted by a mesh of 10 and 18 elements regularly spaced of 454.6 m in both x- and y-direction and of a variable number of vertical layers of 5 m depth in the z-direction. The mesh covers the whole Augusta Harbor and part of the adjacent coastal area. A fixed time step of 300 sec has been chosen to satisfy the several stability conditions and constrains associated to the adopted numerical method (Tveito and Winther, 1998).

The parameters are obtained according to Melaku Canu et al. (2015) and Zhang et al. (2014) (Zhang et al., 2014; Melaku Canu et al., 2015; Horvat et al., 2003), while the components of the velocity field are reproduced for the year 2011 by using the hydrodynamic 3D SHYFEM model (Umgiesser et al., 2004; Umgiesser, 2009). The horizontal and vertical turbulent diffusivities (Pacanowski and Philander, 1981; Denman and Gargett, 1983; Peters et al., 1988; Massel, 1999; Katz et al., 1979; Thi et al., 2005) are calibrated in order to fit the experimental data both for total and dissolved mercury concentrations in seawater and for the mercury fluxes at the 3D domain boundaries.

The photo-demethylation rate constant for methyl-mercury is fixed according to Melaku Canu et al. (2015) (Melaku Canu et al.,

2015; Monperrus et al., 2007b). The photochemical and biological redox reaction rate constants of Hg^0 and Hg^{II} use the parameterizations of Strode et al. (2007), with updates Soerensen at al. (2010) (Zhang et al., 2014; Strode et al., 2007; Soerensen et al., 2010). Specifically, the photochemical oxidation and photochemical reduction first-order rate constants (k_1 and k_2) are directly proportional to the short-wave radiation flux (RAD) at the sea surface attenuated by dissolved organic carbon (DOC) and pigments in the surface ocean (C_{pig}) (Zhang et al., 2014; Soerensen et al., 2010; Qureshi et al., 2010; Batrakova et al., 2014). Also, the biological oxidation and biological reduction first-order rate constants (k_3 and k_4) are directly proportional to the organic carbon remineralization rate (OCRR) of the microbial reactions. Therefore, the photochemical and biological first-order rate constants are calculated as follows:

$$k_1 = k_{photo-ox} \cdot RAD(z), \tag{S2}$$

$$k_2 = k_{photo-red} \cdot RAD(z), \tag{S3}$$

$$k_3 = k_{bio-ox} \cdot OCRR(z), \tag{S4}$$

$$k_4 = k_{bio-red} \cdot OCRR(z), \tag{S5}$$

where $k_{photo-ox}$ and $k_{photo-red}$ are two constants reported by Soerensen at al. (2010) and according to Qureshi et al. (2010), k_{bio-ox} and $k_{bio-red}$ are two constants estimated by Zhang et al. (2014) using the experimental findings of the Hg^0 concentration and net evasion flux in the oceans. The short-wave radiation flux at the water surface ($RAD(0)$) is set up by using the remote sensing data (see the NASA web site http://eosweb.larc.nasa.gov/sse/RETScreen/). The RAD is assumed to decrease exponentially with the depth z, according to the Lambert-Beer's law, and to vary as a function of time t due to the seasonal oscillations of the incident radiation flux $RAD(0)$. The organic carbon remineralization rate, as a function of depth ($OCRR(z)$), is calculated within ($z < z_0$) and out ($z > z_0$) the euphotic zone as follows:

$$OCRR(z) = \frac{NPP}{z_0} \cdot (1 - peratio), \quad if \quad z < z_0 \tag{S6}$$

$$OCRR(z) = -\frac{\partial F_{POC}(z)}{\partial z}, \quad if \quad z > z_0 \tag{S7}$$

where NPP is the net primary production from MODIS satellite data, z_0 is the depth of euphotic zone, $peratio$ is the ratio of the particulate organic carbon concentration (POC) export to NPP out of the euphotic zone, $F_{POC}(z)$ is the sinking flux of POC. Since the bathymetry of the Augusta Bay indicates that the water column depth in the whole basin is less than the euphotic zone depth ($z_0 = 75\ m$), in our model we use only Eq. (S6)). Here, the NPP is set up by using the remote sensing data reported in D'Ortenzio (2003) (D'Ortenzio, 2003), while the $peratio$ is calculated on the basis of the surface atmospheric temperature and the surface chlorophyll concentrations (Zhang et al., 2014) measured in the Augusta basin during the oceanographic survey of May 2011.

S1.1.1 Boundary conditions at the water-atmosphere interface - Dissolved elemental mercury concentration

The mercury flux at the water-atmosphere interface (z=0) is obtained by both the River Model and Bagnato et al. (2013) (Bagnato et al., 2013; Ciffroy, 2015), as follows:

$$\left[D_z \frac{\partial Hg^0}{\partial z} - v_z Hg^0\right]\Big|_{z=0} = \phi_{dep} - \phi_{GEM} = \\ = \frac{Hg_{gas-atm} \cdot Pr}{\Delta t} + MTC_{water-atm} \cdot \left(Hg_{gas-atm} - H \cdot Hg^0|_{z=0}\right), \tag{S8}$$

where

- ϕ_{dep} is the surface deposition flux (dry+wet) of gaseous mercury concentration $[ng \cdot m^{-2} \cdot h^{-1}]$;
- ϕ_{GEM} is the surface evasion flux of elemental mercury concentration $[ng \cdot m^{-2} \cdot h^{-1}]$;
- $Hg_{gas-atm}$ is the gaseous mercury concentration in the atmosphere as a function of time $[ng/l]$;
- Pr is the amount of precipitation as a function of time $[m]$;
- Δt is the exposition time of the basin $[h]$;
- $MTC_{water-atm}$ is the gas phase overall mass transfer coefficient $[m/h]$;
- H is the Henry's law constant $[dimensionless]$.

The temporal behaviour of $Hg_{gas-atm}$ is reproduced for one year by using the experimental data collected by IAS-CNR in 2011, and reported in a previous work (Bagnato et al., 2013). The dynamics of precipitations is obtained by using the remote sensing data on the average monthly precipitations in Augusta Bay (see the NASA web site http://eosweb.larc.nasa.gov/sse/RETScreen/). The $MTC_{water-atm}$ is calculated according to the River model (Ciffroy, 2015) as follows:

$$MTC_{water-atm} = \frac{MTC_{water-atm,w} \cdot MTC_{water-atm,g}}{MTC_{water-atm,w} + H \cdot MTC_{water-atm,g}}. \tag{S9}$$

Here, the water film mass transfer coefficient ($MTC_{water-atm,w}$) and the gas film mass transfer coefficient ($MTC_{water-atm,g}$) are given by:

$$MTC_{water-atm,w} = 0.108 \cdot (u_{wind})^{1.64} \cdot (\frac{PM_{CO_2}}{PM_{molar}})^{0.25}, \tag{S10}$$

$$MTC_{water-atm,g} = 864 \cdot (0.2 \cdot u_{wind} + 0.3) \cdot (\frac{PM_{H_2O}}{PM_{molar}})^{0.3}, \tag{S11}$$

where

- u_{wind} is the wind speed $[m/s]$;
- PM_{CO_2} is the molar mass of carbon dioxide $[g/mol]$;

- PM_{molar} is the molar mass of elemental mercury $[g/mol]$;
- PM_{H_2O} is the molar mass of water $[g/mol]$.

The wind speed is obtained by averaging the values of annual mean wind speed of the last 15 years for the studied area (see the NASA web site http://eosweb.larc.nasa.gov).

The annual mercury evasion flux at the seawater-atmosphere interface (V) is obtained by integrating the ϕ_{GEM} for the whole horizontal surface of the basin, and for the whole year. The annual atmospheric deposition of the elemental mercury is calculated by integrating the ϕ_{dep} for the whole horizontal surface of the basin, and for the whole year.

S1.1.2 Boundary conditions (lateral fluxes) - Dissolved elemental mercury concentration

The lateral fluxes for all variables are set up equal to zero at the boundaries of Augusta basin (Valenti et al., 2017) except where inlets, rivers and sewerage are localized. Moreover, we can neglect the elemental mercury flux at the water-sediment interface ($z = z_b$). Therefore, we fix the following fluxes at the basin boundaries:

$$\left[D_x \frac{\partial Hg^0}{\partial x} - v_x Hg^0\right] = \left[D_y \frac{\partial Hg^0}{\partial y} - v_y Hg^0\right] = \left[D_z \frac{\partial Hg^0}{\partial z} - v_z Hg^0\right]\Big|_{z=z_b} = 0. \tag{S12}$$

For all points of basin where rivers and sewerage are localized, we set:

$$\left[D_x \frac{\partial Hg^0}{\partial x} - v_x Hg^0\right] = INPUT_{x_{point-source}} = \left(\frac{Q_{source}}{A_{source}}\right)\Big|_x \cdot Hg^0_{source} \simeq 0, \tag{S13}$$

$$\left[D_y \frac{\partial Hg^0}{\partial y} - v_y Hg^0\right] = INPUT_{y_{point-source}} = \left(\frac{Q_{source}}{A_{source}}\right)\Big|_y \cdot Hg^0_{source} \simeq 0, \tag{S14}$$

where

- Q_{source} is the average flow rate of water at the point source $[m^3/h]$;
- A_{source} is the longitudinal section of the point source $[m^2]$;
- Hg^0_{source} is the elemental mercury concentration of the point source $[\mu g/m^3]$;
- $INPUT_{x_{point-source}}$ and $INPUT_{y_{point-source}}$ are the fluxes of elemental mercury $[\mu g \cdot m^{-2} \cdot h^{-1}]$ along x-direction and y-direction, respectively, entering the basin from the point source.

The lateral fluxes at inlets (Scirocco and Levante) of the basin (Salvagio Manta et al., 2016) (Sprovieri et al., 2011; Sprovieri, 2015; Salvagio Manta et al., 2016) as a function of depth and time are given by:

$$\begin{aligned}\phi^0_{x_{inlet}}(z,t) &= \left[D_x \tfrac{\Delta Hg^0}{\Delta x} - v_{x_{inlet}}(z,t) \cdot Hg^0_{ext}(z)\right] = \\ &= \left[D_x \tfrac{\Delta Hg^0}{\Delta x} + v_{x_{inlet}}(z,t) \cdot Hg^0_{int}(z,t)\right],\end{aligned} \tag{S15}$$

$$\phi^0_{y_{inlet}}(z,t) = \left[D_y \frac{\Delta Hg^0}{\Delta y} - v_{y_{inlet}}(z,t) \cdot Hg^0_{ext}(z)\right] = \\ = \left[D_y \frac{\Delta Hg^0}{\Delta y} + v_{y_{inlet}}(z,t) \cdot Hg^0_{int}(z,t)\right], \tag{S16}$$

where

- $v_{x_{inlet}}(z,t)$ is the absolute value of the marine currents velocity at the inlet along the x-direction $[m/h]$;
- $v_{y_{inlet}}(z,t)$ is the absolute value of the marine currents velocity at the inlet along the y-direction $[m/h]$;
- $Hg^0_{int}(z,t)$ ($Hg^0_{ext}(z)$) is the internal (external) dissolved elemental mercury concentrations close to the inlet $[\mu g/m^3]$;
- ΔHg^0 is the difference between the internal and external dissolved elemental mercury concentrations at the inlet of basin $[\mu g/m^3]$;
- $\phi^0_{x_{inlet}}(z,t)$ and $\phi^0_{y_{inlet}}(z,t)$ are the horizontal fluxes at the inlet $[\mu g \cdot m^{-2} \cdot h^{-1}]$.

The advection terms of Eqs. (S15)-(S16) are negative when the marine current velocities cause the external seawater to enter into the Augusta Bay, while they are positive when the marine current velocities cause the internal seawater to come out the basin. The annual net outflow of elemental mercury from basin to open sea is obtained by integrating Eqs. (S15)-(S16) for the whole lateral surface of the two inlets, and for the whole year.

S1.2 Dissolved inorganic mercury concentration

The dynamics of the dissolved inorganic mercury concentration (Hg^{II}) within the 3-D domain of the Augusta basin (Han et al., 2007; Whalin et al., 2007; Monperrus et al., 2007b; Zhang et al., 2014; Batrakova et al., 2014; Melaku Canu et al., 2015; Salvagio Manta et al., 2016) is described by the following PDE:

$$\begin{aligned} \frac{\partial Hg^{II}}{\partial t} = \; & + \frac{\partial}{\partial x}\left[D_x \frac{\partial Hg^{II}}{\partial x}\right] - \frac{\partial}{\partial x}(v_x Hg^{II}) + \frac{\partial}{\partial y}\left[D_y \frac{\partial Hg^{II}}{\partial y}\right] - \frac{\partial}{\partial y}(v_y Hg^{II}) \\ & + \frac{\partial}{\partial z}\left[D_z \frac{\partial Hg^{II}}{\partial z}\right] - \frac{\partial}{\partial z}(v_z Hg^{II}) + (k_1 + k_3) \cdot Hg^0 - (k_2 + k_4) \cdot Hg^{II} - k_{me} \cdot Hg^{II} \\ & + S^{II}_L + S^{II}_{DOM} - S^{II}_{SPM}, \end{aligned} \tag{S17}$$

where

- k_{me} is the rate constant for the methylation of inorganic mercury $[1/h]$;
- S^{II}_L is the direct loads of the inorganic mercury $[ng \cdot l^{-1} \cdot h^{-1}]$;
- S^{II}_{DOM} is the load of the dissolved inorganic mercury released by the particulate organic matter $[ng \cdot l^{-1} \cdot h^{-1}]$;
- S^{II}_{SPM} is the adsorption rate of the suspended particulate matter for the dissolved inorganic mercury $[ng \cdot l^{-1} \cdot h^{-1}]$.

The integration domain of the PDE is constituted by a mesh of 10 and 18 elements regularly spaced of 454.6 m in both x- and y-direction and of a variable number of vertical layers of 5 m depth in the z-direction. The mesh covers the whole Augusta Harbor and part of the adjacent coastal area. A fixed time step of 300 sec has been chosen to satisfy the several stability conditions and constrains associated to the adopted numerical method (Tveito and Winther, 1998).

The rate constant for the methylation of inorganic mercury is fixed according to Monperrus et al. (2007) (Batrakova et al., 2014; Monperrus et al., 2007b). The other rate constants of Eq. (S17) are defined in the section 1.1 (Zhang et al., 2014; Strode et al., 2007; Soerensen et al., 2010; Qureshi et al., 2010; Batrakova et al., 2014; Melaku Canu et al., 2015; Monperrus et al., 2007b).

The load of dissolved inorganic mercury released by particulate organic matter (S^{II}_{DOM}) is given by:

$$S^{II}_{DOM} = \quad \lambda \cdot m \cdot b \cdot PHg^{II}, \tag{S18}$$

where

- PHg^{II} is the inorganic mercury mass accumulated in each cell of eukaryotes population $[\mu g/cell]$;
- b is the cell concentration of eukaryotes population $[cell/m^3]$;
- m is the mortality of eukaryotes population $[h^{-1}]$

All parameters and variables of Eq. (S18) are defined in the Phytoplankton model and NP model (see sections 4 and 5) except λ, which is the mercury recycling coefficient for the eukaryotes population (Ciffroy, 2015; Dutkiewicz et al., 2009; Morozov et al., 2010; Valenti et al., 2012; Denaro et al., 2013a, c, b; Valenti et al., 2015, 2016a, b, c, 2017).

The adsorption rate of the suspended particulate matter for the dissolved inorganic mercury (S^{II}_{SPM}) is obtained by Zhang et al. (2014) (Zhang et al., 2014), as follows:

$$S^{II}_{SPM} = \quad -\frac{\partial}{\partial z}\left[NPP \cdot (peratio) \cdot \left(\frac{z}{z_0}\right)^{-0.9} \cdot \left(\frac{k_D}{f_{org}}\right) \cdot Hg^{II}(z)\right], \tag{S19}$$

where

- NPP is the net primary production $[mol\ \ C \cdot m^{-2} \cdot h^{-1}]$;
- $peratio$ is the ratio of particulate organic carbon (POC) export to NPP out of the euphotic zone $[dimensionless]$;
- k_D is the water-SPM partition coefficient for dissolved mercury $[l/Kg]$;
- f_{org} is the organic fraction of suspended particulate matter in dissolved-phase $[dimensionless]$, which takes on a different value in each position (x,y) of the domain;
- z_0 is the depth of euphotic zone $[m]$.

The NPP is set up by using the remote sensing data reported in previous work (D'Ortenzio, 2003). The spatial distribution of f_{org} is reproduced by using the SPOM and SPM concentrations measured in the Augusta Bay during the oceanographic survey of October 2017. The partition coefficient k_D is calibrated in such a way to obtain the best fit with the experimental data for total and dissolved mercury concentrations in the seawater compartment. The $peratio$ is calculated by using the following equation (Zhang et al., 2014):

$$peratio = -0.0081 \cdot T + 0.0806 \ln Chl + 0.426, \quad \text{(S20)}$$

where T is the surface atmospheric temperature (C) and Chl is the surface chlorophyll concentration ($mg\ m^{-3}$). The former is obtained from remote sensing data. The latter is set on the basis of the values measured in Augusta basin during the oceanographic survey of May 2011.

The dissolved inorganic mercury concentration as a function of depth ($Hg^{II}(z)$) is obtained by solving Eq. (S17). Since the adsorption rate of the SPM for the dissolved inorganic mercury (S^{II}_{SPM}) has to vanish at $z = 0$ due to the condition of "cleaned" SPM entering through the seawater surface, in the Eq. (S19) we fix the dissolved inorganic mercury concentration equal to zero at the seawater-atmosphere interface ($Hg^{II}(0) = 0$).

The annual amount of inorganic mercury removed by the suspended particulate along the water column (scavenging process) is obtained by integrating Eq. (S19) on the whole 3D domain of the Augusta Bay.

S1.2.1 Boundary conditions at the water-atmosphere interface - Dissolved inorganic mercury concentration

The inorganic mercury flux at the water-atmosphere interface (z=0) is calculated by the River Model and Bagnato et al. (2013) (Bagnato et al., 2013; Ciffroy, 2015), as follows:

$$\left[D_z \frac{\partial Hg^{II}}{\partial z} - v_z Hg^{II}\right]\Big|_{z=0} = Wetdep_{part} + Wetdep_{gas} + Drydep_{part} = \frac{Hg^{II}_{atm} \cdot Pr}{\Delta t}, \quad \text{(S21)}$$

where

- $Wetdep_{part}$ is the surface wet deposition flux of contaminated particles $[ng \cdot m^{-2} \cdot h^{-1}]$;
- $Wetdep_{gas}$ is the surface wet deposition flux of contaminated gas $[ng \cdot m^{-2} \cdot h^{-1}]$;
- $Drydep_{part}$ is the surface dry deposition flux of contaminated particles $[ng \cdot m^{-2} \cdot h^{-1}]$;
- Hg^{II}_{atm} is the inorganic mercury concentration in atmosphere as a function of time $[ng/m^3]$;
- Pr is the amount of precipitation as a function of time $[m]$;
- Δt is the exposition time of the basin $[h]$.

The time behaviour of the inorganic mercury concentration in atmosphere (Hg^{II}_{atm}) is reproduced for one year by using the experimental data collected reported in a previous work (Bagnato et al., 2013). The dynamics of precipitations is obtained by using the remote sensing data on the average monthly precipitations in Augusta Bay (see the NASA web site

http://eosweb.larc.nasa.gov).

The annual atmospheric deposition of the inorganic mercury is calculated by integrating Eq. (S21) for the whole horizontal surface of the basin and for the whole year. The annual total atmospheric mercury deposition (AD) is equal to the sum of the amounts of inorganic and elemental mercury deposited on the surface of the Augusta basin in one year.

S1.2.2 Boundary conditions at the water-sediment interface - Dissolved inorganic mercury concentration

The inorganic mercury flux at the water-sediment interface ($z = z_b$) is calculated as a function of time in each position (x,y) of the domain (River Merlin-Expo model, 2015) (Covelli et al., 2008; Ciffroy, 2015):

$$\begin{aligned}\left[D_z \frac{\partial Hg^{II}}{\partial z} - v_z Hg^{II}\right]\Big|_{z=z_b} &= MTC^{II}_{sed-water} \cdot \left(Hg^{II}_{pore-water} - Hg^{II}_{dis-water}\right) + \phi^{II}_{res} = \\ &= MTC^{II}_{sed-water} \cdot \left(Hg^{II}_{pore-water} - Hg^{II}_{dis-water}\right) + Hg^{II}_{pore-water} \cdot \varphi_{sed} \cdot Er,\end{aligned} \tag{S22}$$

where

- $MTC^{II}_{sed-water}$ is the mass transfer coefficient for the inorganic mercury at the water-sediment interface $[m/h]$, which takes on a different value in each position (x,y) of the domain;
- $Hg^{II}_{pore-water}$ is the inorganic mercury concentration in the pore water of the shallowest layer of the sediment $[\mu g/m^3]$;
- ϕ^{II}_{res} is the inorganic mercury flux at the seawater-sediment interface caused by the particulate matter deposition-resuspension process $[\mu g/m^2 h]$;
- φ_{sed} is the porosity of the sediment $[dimensionless]$;
- Er is the removed/settled sediment thickness at the seawater-sediment interface as a function of position (x,y) and time $[m/h]$;
- $Hg^{II}_{dis-water}$ is the dissolved inorganic mercury concentration in the deepest layer of the seawater $[\mu g/m^3]$;
- z_b is the depth of the water column $[m]$ in each position (x,y).

The annual benthic flux of inorganic mercury ($R_{Hg^{II}}$) is obtained by integrating Eq. (S22) for the whole horizontal surface of the basin, and for the whole year.

The mass transfer coefficient for the inorganic mercury at the water-sediment interface ($MTC^{II}_{sed-water}$) (Ciffroy, 2015) is calculated as follows:

$$MTC^{II}_{sed-water} = \frac{D_{w-in} \cdot \varphi^{4/3}_{sed}}{\delta^{II}_{sed} + \delta_w \cdot \varphi^{4/3}_{sed}}, \tag{S23}$$

where

- D_{w-in} is the molecular diffusion coefficient for the inorganic mercury $[m^2/h]$;

- φ_{sed} is the porosity of the sediment $[dimensionless]$;
- δ_{sed}^{II} is the boundary layer thickness above the sediment for the inorganic mercury $[m]$;
- δ_w is the boundary layer thickness below sediment $[m]$.

The molecular diffusion coefficient is that reported by Schulz and Zabel (2006) (Schulz and Zabel, 2006), while the porosity of the sediment is calculated using the values of specific weight and humidity reported in the study of ICRAM (2008) (Mare, 2008). The *boundary layer thickness below the sediment* is obtained by the marine currents velocities at the seawater-sediment interface, according to previous works (Ciffroy, 2015; Sørensen et al., 2001). Finally, the *boundary layer thickness above the sediment for the inorganic mercury* is calibrated on the basis both of the vertical fluxes and the dissolved mercury concentration measured close to the seabed during the oceanographic surveys of September 2011 and June 2012 (Salvagio Manta et al., 2016).

Unlike the mass transfer coefficient for the inorganic mercury at the water-sediment interface ($MTC_{sed-water}^{II}$), the mass transfer coefficient for the inorganic mercury within the sediment is estimated by considering an alternative mechanism for the mercury diffusion in the pore water, in accordance with recent works (Schulz and Zabel, 2006) (Schulz and Zabel, 2006). Initially we calculate the molecular diffusion coefficient for the inorganic mercury in the pore water of the sediment (D_{sed}^{in}) as follows:

$$D_{sed}^{in} = \varphi_{sed} \cdot \frac{D_{w-in}}{\theta^2} = \frac{\varphi_{sed} \cdot D_{w-in}}{1 - ln(\varphi_{sed}^2)}, \tag{S24}$$

where θ is the tortuosity of the sediment $(dimensionless)$.

According to Melaku Canu et al. (2015) and Oliveri et al. (2016) (Melaku Canu et al., 2015; Oliveri et al., 2016), we calculate the inorganic mercury concentration in the pore water and the total mercury concentration in the sediment as a function of time, by using the following differential equations:

$$\begin{aligned} \frac{dHg_{pore-water}^{II}}{dt} &= +K_{demeth} \cdot MeHg_{pore-water} - K_{meth} \cdot Hg_{pore-water}^{II} + \frac{\partial}{\partial x}\left[D_{sed}^{in} \cdot \frac{\partial Hg_{pore-water}^{II}}{\partial x}\right] \\ &+ \frac{\partial}{\partial y}\left[D_{sed}^{in} \cdot \frac{\partial Hg_{pore-water}^{II}}{\partial y}\right] + \frac{\partial}{\partial z}\left[D_{sed}^{in} \cdot \frac{\partial Hg_{pore-water}^{II}}{\partial z}\right] - \frac{(1-k_{MeHg})}{K_d^{II}} \cdot \frac{dHg_T^{sed}}{dt} \\ \frac{dHg_T^{sed}}{dt} &= -\alpha \cdot Hg_T^{sed} \Rightarrow Hg_T^{sed}(t) = Hg_T^{sed}(0) \cdot exp(-\alpha \cdot t), \ \ with \ \ \alpha > 0, \end{aligned} \tag{S25}$$

where

- K_{demeth} is the rate constant for the de-methylation of methyl-mercury in the pore water of the sediment $[1/h]$;
- K_{meth} is the rate constant for the methylation of inorganic mercury in the pore water of the sediment $[1/h]$;
- $MeHg_{pore-water}$ is the methyl-mercury concentration in the pore water of the sediment $[\mu g/m^3]$;
- α is the de-adsorption rate (constant) for the total mercury concentration in the sediment $[1/h]$;
- k_{MeHg} is the fraction of methyl-mercury in the sediment $[dimensionless]$;

– K_d^{II} is the sediment-pore water distribution coefficient for the inorganic mercury $[l/Kg]$.

The rates of the first equation, except α, have been estimated for the Gulf of Trieste by Melaku Canu et al. (2015) (Melaku Canu et al., 2015; Hines et al., 2012; Monperrus et al., 2007a), while the fraction of methyl-mercury in the sediment has been measured during the oceanographic survey of October 2017. The sediment-pore water distribution coefficient for the inorganic mercury is calibrated, according to previous works (Melaku Canu et al., 2015; Liu et al., 2012; Oliveri et al., 2016), in such a way to better reproduce the real inorganic mercury concentration measured in the pore water. Finally, the de-adsorption rate for the total mercury concentration and the sediment-pore water distribution coefficient for the inorganic mercury have been calibrated on the basis of the mercury concentration measured experimentally in the samples of pore water collected in May 2011 (Oliveri et al., 2016).

S1.2.3 Initial conditions for the inorganic mercury concentration in pore water

In general, the inorganic mercury concentration in pore water is estimated by the total mercury concentration (Hg_T^{sed}) and the sediment-pore water distribution coefficient (K_d^{II}) (Cossa and Coquery, 2005; Sunderland et al., 2006; Hines et al., 2012; Monperrus et al., 2007a). On this basis, we fix the initial condition (t=0) for the inorganic mercury concentration in pore water using the following equation:

$$Hg_{pore-water}^{II}(0) = (1 - k_{MeHg}) \cdot \frac{Hg_T^{sed}(0)}{K_d^{II}}, \tag{S26}$$

where $THg_{sed}(0)$ is the total mercury concentration in the sediment at $t = 0$ (initial condition) $[mg/Kg]$, with different values in each position (x,y,z) of the domain. This is estimated in the 3D domain of the Augusta Bay by interpolating the experimental data collected by ICRAM during the oceanographic survey performed in the period 2005-2006 (Mare, 2008).

S1.2.4 Initial conditions for the total mercury concentration, specific weight and humidity in the sediments. Interpolation methods

The spatial distribution of total mercury, specific weight and percentage of the humidity of the sediments of the Augusta Bay were estimated within the whole study area in order to simulate mercury flux at the sediment/water interface and between sediment layers. The vertical profiles of these variables were interpolated through Inverse Distance Weighting (IDW) on transects of points of a mesh 18×10 with 454.6 m of distance between the nodes, able to cover the entire investigated area. The values corresponding to the nodes at depth 10 cm, 30 cm, 50 cm, 90 cm, 110 cm, 130 cm, 150 cm, 170 cm and 190 cm were extracted and included as input data in the mathematical model.

S1.2.5 Boundary conditions (lateral fluxes) - Dissolved inorganic mercury concentration

The Augusta basin can be considered as closed except for the inlets, rivers and sewerage (Valenti et al., 2017). Therefore, we fix the following lateral fluxes at the boundaries of the domain:

$$\left[D_x \frac{\partial Hg^{II}}{\partial x} - v_x Hg^{II}\right] = \left[D_y \frac{\partial Hg^{II}}{\partial y} - v_y Hg^{II}\right] = 0. \tag{S27}$$

For all points of basin where rivers and sewerage are localized, we set:

$$\left[D_x \frac{\partial Hg^{II}}{\partial x} - v_x Hg^{II}\right] = INPUT_{x_{point-source}} = \left(\frac{Q_{source}}{A_{source}}\right)\Big|_x \cdot Hg^{II}_{source} \simeq 0, \tag{S28}$$

$$\left[D_y \frac{\partial Hg^{II}}{\partial y} - v_y Hg^{II}\right] = INPUT_{y_{point-source}} = \left(\frac{Q_{source}}{A_{source}}\right)\Big|_y \cdot Hg^{II}_{source} \simeq 0, \tag{S29}$$

where

- Q_{source} is the average flow rate of water for the point source $[m^3/h]$;
- A_{source} is the longitudinal section of the point source $[m^2]$;
- Hg^{II}_{source} is the mercury concentration of the point source $[\mu g/m^3]$;
- $INPUT_{x_{point-source}}$ and $INPUT_{y_{point-source}}$ are the fluxes of inorganic mercury $[\mu g \cdot m^{-2} \cdot h^{-1}]$ along x-direction and y-direction, respectively, entering the basin from the point source.

The lateral fluxes of inorganic mercury concentration at inlets (Scirocco and Levante) of the basin (Salvagio Manta et al., 2016) (Sprovieri et al., 2011; Sprovieri, 2015; Salvagio Manta et al., 2016) as a function of depth and time are given by:

$$\begin{aligned}\phi^{II}_{x_{inlet}}(z,t) &= \left[D_x \tfrac{\Delta Hg^{II}}{\Delta x} - v_{x_{inlet}}(z,t) \cdot Hg^{II}_{ext}(z)\right] = \\ &= \left[D_x \tfrac{\Delta Hg^{II}}{\Delta x} + v_{x_{inlet}}(z,t) \cdot Hg^{II}_{int}(z,t)\right],\end{aligned} \tag{S30}$$

$$\begin{aligned}\phi^{II}_{y_{inlet}}(z,t) &= \left[D_y \tfrac{\Delta Hg^{II}}{\Delta y} - v_{y_{inlet}}(z,t) \cdot Hg^{II}_{ext}(z)\right] = \\ &= \left[D_y \tfrac{\Delta Hg^{II}}{\Delta y} + v_{y_{inlet}}(z,t) \cdot Hg^{II}_{int}(z,t)\right],\end{aligned} \tag{S31}$$

where

- $v_{x_{inlet}}(z,t)$ is the absolute value of the marine currents velocity at the inlet along the x-direction $[m/h]$;
- $v_{y_{inlet}}(z,t)$ is the absolute value of the marine currents velocity at the inlet along the y-direction $[m/h]$;
- $Hg^{II}_{int}(z)$ ($Hg^{II}_{ext}(z)$) is the internal (external) dissolved inorganic mercury concentrations close to the inlet $[\mu g/m^3]$;
- ΔHg^{II} is the difference between the internal and external dissolved inorganic mercury concentrations at the inlet of basin $[\mu g/m^3]$;
- $\phi^{II}_{x_{inlet}}(z,t)$ and $\phi^{II}_{y_{inlet}}(z,t)$ are the horizontal fluxes of inorganic mercury concentration at the inlet $[\mu g \cdot m^{-2} \cdot h^{-1}]$.

The advection terms of Eqs. (S30)-(S31) are negative when the marine current velocities cause the external seawater to enter the Augusta Bay, while they are positive when the marine current velocities cause the internal seawater to come out from the basin. The annual net outflow of inorganic mercury from basin to open sea is obtained by integrating Eqs. (S30)-(S31) for the whole lateral surface of the two inlets and for the whole year.

S1.3 Dissolved methyl-mercury concentration

On the basis of the overall equation for the mass conservation of the state variables in dissolved phase (Han et al., 2007; Whalin et al., 2007; Monperrus et al., 2007b; Zhang et al., 2014; Batrakova et al., 2014; Melaku Canu et al., 2015; Salvagio Manta et al., 2016), the dynamics of dissolved methyl-mercury concentration ($MeHg$) within the 3-D domain of Augusta basin is described by the following PDE:

$$\begin{aligned}\frac{\partial MeHg}{\partial t} = \quad & +\frac{\partial}{\partial x}\left[D_x\frac{\partial MeHg}{\partial x}\right]-\frac{\partial}{\partial x}(v_x MeHg)+\frac{\partial}{\partial y}\left[D_y\frac{\partial MeHg}{\partial y}\right]-\frac{\partial}{\partial y}(v_y MeHg)\\ & +\frac{\partial}{\partial z}\left[D_z\frac{\partial MeHg}{\partial z}\right]-\frac{\partial}{\partial z}(v_z MeHg)-k_{Ph-de}\cdot MeHg+k_{me}\cdot Hg^{II}\\ & +S_L^{MM}+S_{DOM}^{MM}-S_{SPM}^{MM},\end{aligned} \tag{S32}$$

where

- S_L^{MM} is the direct loads of methyl-mercury $[ng\cdot l^{-1}\cdot h^{-1}]$;
- S_{DOM}^{MM} is the load of dissolved methyl-mercury released by particulate organic matter $[ng\cdot l^{-1}\cdot h^{-1}]$;
- S_{SPM}^{MM} is the adsorption rate of suspended particulate matter for dissolved methyl-mercury $[ng\cdot l^{-1}\cdot h^{-1}]$.

The integration domain of the PDE is constituted by a mesh of 10 and 18 elements regularly spaced of 454.6 m in both x- and y-direction and of a variable number of vertical layers of 5 m depth in the z-direction. The mesh covers the whole Augusta Harbor and part of the adjacent coastal area. A fixed time step of 300 sec has been chosen to satisfy the several stability conditions and constrains associated to the adopted numerical method (Tveito and Winther, 1998).

The rate constant for the methylation of inorganic mercury is fixed according to Monperrus et al. (2007) (Batrakova et al., 2014; Monperrus et al., 2007b). The rate constant for the photo-demethylation of methyl-mercury (k_{Ph-de}) is defined in section 1.1 (Zhang et al., 2014; Batrakova et al., 2014; Melaku Canu et al., 2015; Monperrus et al., 2007b).

The load of dissolved methyl-mercury released by the particulate organic matter (S_{DOM}^{MM}) is given by:

$$S_{DOM}^{MM} = \quad \lambda\cdot m\cdot b\cdot PMeHg, \tag{S33}$$

where

- $PMeHg$ is the methyl-mercury mass accumulated in each cell of the eukaryotes population $[\mu g/cell]$;
- b is the cell concentration of eukaryotes population $[cell/m^3]$;
- m is the mortality of eukaryotes population $[h^{-1}]$.

All parameters and variables of Eq. (S33) are defined in the Phytoplankton model and NP model (see sections 4 and 5) except λ, which is the mercury recycling coefficient for the eukaryotes population (Ciffroy, 2015; Dutkiewicz et al., 2009; Morozov et al., 2010; Valenti et al., 2012; Denaro et al., 2013a, c, b; Valenti et al., 2015, 2016a, b, c, 2017).

The adsorption rate of the suspended particulate matter for the dissolved organic mercury (S_{SPM}^{MM}) is obtained in agrement with Zhang et al. (2014) (Zhang et al., 2014), as follows:

$$S_{SPM}^{MM} = -\frac{\partial}{\partial z}\left[NPP \cdot (peratio) \cdot \left(\frac{z}{z_0}\right)^{-0.9} \cdot \left(\frac{k_D}{f_{org}}\right) \cdot MeHg(z)\right], \tag{S34}$$

where

- NPP is the net primary production $[mol\ \ C \cdot m^{-2} \cdot h^{-1}]$;
- $peratio$ is the ratio of particulate organic carbon (POC) export to NPP out of the euphotic zone $[dimensionless]$;
- k_D is the water-SPM partition coefficient for the dissolved mercury $[l/Kg]$;
- z_0 is the depth of the euphotic zone $[m]$.

The NPP is set by using the remote sensing data reported in a previous work (D'Ortenzio, 2003). The spatial distribution of f_{org} is reproduced by using the SPOM and SPM concentrations measured in the Augusta Bay during the oceanographic survey of October 2017. The partition coefficient k_D is calibrated in such a way to obtain the best fit between theoretical results and experimental data for total and dissolved mercury concentrations in the seawater compartment. The $peratio$ is calculated by using Eq. (S20) (see section 1.2).

The dissolved methyl-mercury concentration as a function of depth ($MeHg(z)$) is obtained by solving Eq. (S32). Since the adsorption rate of the SPM for the dissolved methyl-mercury (S_{SPM}^{II}) has to vanish at $z = 0$ because of the condition of "cleaned" SPM entering at seawater surface, in the Eq. (S34) we fix the dissolved methyl-mercury concentration equal to zero at the seawater-atmosphere interface ($MeHg(0) = 0$).

The annual amount of methyl-mercury removed by the suspended particulate along the water column (scavenging process) is obtained by integrating Eq. (S34) on the whole 3D domain of the Augusta Bay, as well as for the inorganic mercury. The annual total mercury flux recycled for scavenging (S) is equal to the sum of the amounts of inorganic mercury and methyl-mercury adsorbed by the SPM along the water column in one year.

S1.3.1 Boundary conditions at the water-atmosphere interface - Dissolved methyl-mercury concentration

The methyl-mercury flux at the water-atmosphere interface (z=0) can be neglected because the methyl-mercury concentration is very low in atmosphere ($MeHg_{atm} \simeq 0$). Therefore, according to the River Model and Bagnato et al. (2013) (Ciffroy, 2015; Bagnato et al., 2013), we set:

$$\left[D_z \frac{\partial MeHg}{\partial z} - v_z MeHg\right]\Big|_{z=0} = Wetdep_{part} + Wetdep_{gas} + Drydep_{part} = \frac{MeHg_{atm} \cdot Pr}{\Delta t} = 0, \tag{S35}$$

where

- $Wetdep_{part}$ is the surface wet deposition flux of contaminated particles $[ng \cdot m^{-2} \cdot h^{-1}]$;
- $Wetdep_{gas}$ is the surface wet deposition flux of contaminated gas $[ng \cdot m^{-2} \cdot h^{-1}]$;

- $Drydep_{part}$ is the surface dry deposition flux of contaminated particles $[ng \cdot m^{-2} \cdot h^{-1}]$;
- $MeHg_{atm}$ is the methyl-mercury concentration in atmosphere as a function of time $[ng/m^3]$;
- Pr is the amount of precipitation as a function of time $[m]$;
- Δt is the exposition time of the basin $[h]$.

The methyl-mercury concentration in atmosphere ($MeHg_{atm}$) is assumed to be equal to zero for the whole year, according to Driscoll et al.(2013) (Driscoll et al., 2013). The dynamics of precipitations is obtained by using the remote sensing data on the average monthly precipitations in Augusta Bay (see the NASA web site http://eosweb.larc.nasa.gov).
The annual atmospheric deposition of the methyl-mercury is set equal to zero since the methyl-mercury concentration in atmosphere ($MeHg_{atm}$) is assumed negligible.

S1.3.2 Boundary conditions at the water-sediment interface - Dissolved methyl-mercury concentration

The methyl-mercury flux at the water-sediment interface ($z = z_b$) is calculated as a function of time in each position (x,y) of the domain (River Merlin-Expo model, 2015) (Covelli et al., 2008; Ciffroy, 2015):

$$\begin{aligned}\left[D_z \frac{\partial MeHg}{\partial z} - v_z MeHg\right]\Big|_{z=z_b} &= MTC^{MM}_{sed-water} \cdot (MeHg_{pore-water} - MeHg_{dis-water}) + \phi^{MM}_{res} = \\ &= MTC^{MM}_{sed-water} \cdot (MeHg_{pore-water} - MeHg_{dis-water}) + MeHg_{pore-water} \cdot \varphi_{sed} \cdot Er,\end{aligned} \tag{S36}$$

where

- $MTC^{MM}_{sed-water}$ is the mass transfer coefficient for the methyl-mercury at the water-sediment interface $[m/h]$, which takes on a different value in each position (x,y) of the domain;
- $MeHg_{pore-water}$ is the methyl-mercury concentration in the pore water of the shallowest layer of the sediment $[\mu g/m^3]$;
- ϕ^{MM}_{res} is the methyl-mercury flux at the seawater-sediment interface caused by the particulate matter deposition-resuspension process $[\mu g/m^2 h]$;
- φ_{sed} is the porosity of the sediment $[dimensionless]$;
- Er is the removed/settled sediment thickness at the seawater-sediment interface as a function of position (x,y) and time $[m/h]$;
- $MeHg_{dis-water}$ is the dissolved methyl-mercury concentration in the deepest layer of seawater $[\mu g/m^3]$;
- z_b is the depth of the water column $[m]$ in each position (x,y).

The annual benthic flux of methyl-mercury (R_{MeHg}) is obtained by integrating Eq. (S36) for the whole horizontal surface of the basin and for the whole year. The annual mercury benthic flux (R) is equal to the sum of the amounts of inorganic mercury

and methyl-mercury released from the sediments of the Augusta Bay in one year.

The mass transfer coefficient for the methyl-mercury at the water-sediment interface ($MTC^{MM}_{sed-water}$) (Ciffroy, 2015) is calculated as follows:

$$MTC^{MM}_{sed-water} = \frac{D_{w-or} \cdot \varphi^{4/3}_{sed}}{\delta^{MM}_{sed} + \delta_w \cdot \varphi^{4/3}_{sed}}, \tag{S37}$$

where

- D_{w-or} is the molecular diffusion coefficient for the methyl-mercury $[m^2/h]$;
- φ_{sed} is the porosity of the sediment $[dimensionless]$;
- δ^{MM}_{sed} is the boundary layer thickness above the sediment for the methyl-mercury $[m]$;
- δ_w is the boundary layer thickness below the sediment $[m]$.

The molecular diffusion coefficient is that reported by Schulz and Zabel (2006) (Schulz and Zabel, 2006), while the porosity of the sediment is calculated by using the values of specific weight and humidity reported in the study of ICRAM (2008) (Mare, 2008). The *boundary layer thickness below the sediment* is obtained by the marine currents velocities at the seawater-sediment interface, according to the previous works (Ciffroy, 2015; Sørensen et al., 2001). Finally, the *boundary layer thickness above the sediment for the methyl-mercury* is calibrated on the basis both of the vertical fluxes and the methyl-mercury concentration measured close to the seabed during the oceanographic surveys of September 2011 and June 2012 (Salvagio Manta et al., 2016).

Unlike the mass transfer coefficient for the methyl-mercury at the water-sediment interface ($MTC^{MM}_{sed-water}$), the mass transfer coefficient for the methyl-mercury in sediment is estimated by considering an alternative mechanism for the mercury diffusion in the pore water, in agreement with recent works (Schulz and Zabel, 2006) (Schulz and Zabel, 2006). Therefore, initially we calculate the molecular diffusion coefficient for the methyl-mercury in the pore water of the sediment (D^{or}_{sed}) as follows:

$$D^{or}_{sed} = \varphi_{sed} \cdot \frac{D_{w-or}}{\theta^2} = \frac{\varphi_{sed} \cdot D_{w-or}}{1 - ln(\varphi^2_{sed})}, \tag{S38}$$

where θ is the tortuosity of the sediment $(dimensionless)$.

Than, according to Melaku Canu et al. (2015) and Oliveri et al. (2016) (Melaku Canu et al., 2015; Oliveri et al., 2016), we calculate the methyl-mercury concentration in the pore water and the total mercury concentration in the sediment as a function of time, by considering the molecular diffusion within the sediment, as follows:

$$\begin{aligned} \tfrac{dMeHg_{pore-water}}{dt} &= -K_{demeth} \cdot MeHg_{pore-water} + K_{meth} \cdot Hg^{II}_{pore-water} + \tfrac{\partial}{\partial x}\left[D^{or}_{sed} \cdot \tfrac{\partial MeHg_{pore-water}}{\partial x}\right] \\ &+ \tfrac{\partial}{\partial y}\left[D^{or}_{sed} \cdot \tfrac{\partial MeHg_{pore-water}}{\partial y}\right] + \tfrac{\partial}{\partial z}\left[D^{or}_{sed} \cdot \tfrac{\partial MeHg_{pore-water}}{\partial z}\right] - \tfrac{k_{MeHg}}{K^{MM}_d} \cdot \tfrac{dHg^{sed}_T}{dt} \\ \tfrac{dHg^{sed}_T}{dt} &= -\alpha \cdot Hg^{sed}_T \Rightarrow Hg^{sed}_T(t) = Hg^{sed}_T(0) \cdot exp(-\alpha \cdot t), \;\; with \;\; \alpha > 0, \end{aligned} \tag{S39}$$

where

- K_{demeth} is the rate constant for the de-methylation of methyl-mercury in the pore water of the sediment $[1/h]$;
- K_{meth} is the rate constant for the methylation of inorganic mercury in the pore water of the sediment $[1/h]$;
- $Hg^{II}_{pore-water}$ is the inorganic mercury concentration in the pore water of the sediment $[\mu g/m^3]$;
- α is the de-adsorption rate (constant) for the total mercury concentration in the sediment $[1/h]$;
- k_{MeHg} is the fraction of the methyl-mercury in the sediment $[dimensionless]$;
- K^{MM}_d is the sediment - pore water distribution coefficient for methyl-mercury $[l/Kg]$.

The rates of the first equation, except α, have been estimated for the Gulf of Trieste by Melaku Canu et al. (2015) (Melaku Canu et al., 2015; Hines et al., 2012; Monperrus et al., 2007a), while the fraction of the methyl-mercury in the sediment has been measured during the oceanographic survey of October 2017. The sediment-pore water distribution coefficient for the methyl-mercury is fixed equal to the square root of the distribution coefficient for the inorganic mercury, according to Liu et al. (2012) (Liu et al., 2012). Finally, the sediment-pore water distribution coefficient for the methyl-mercury is calibrated on the basis of the mercury concentration measured experimentally in the samples of the pore water collected in May 2011 (Oliveri et al., 2016).

S1.3.3 Initial conditions for methyl-mercury concentration in the pore water

In general, the methyl-mercury concentration in the pore water is estimated by the total mercury concentration (Hg^{sed}_T) and the sediment-pore water distribution coefficient (K^{MM}_d) (Cossa and Coquery, 2005; Sunderland et al., 2006; Hines et al., 2012; Monperrus et al., 2007a). On this basis, we fix the initial condition (t=0) for the methyl-mercury concentration in the pore water by using the following equation:

$$MeHg_{pore-water}(0) = k_{MeHg} \cdot \frac{Hg^{sed}_T(0)}{K^{MM}_d}. \tag{S40}$$

where $THg_{sed}(0)$ is the total mercury concentration in the sediment at t=0 (initial condition) $[mg/Kg]$, which takes on a different value in each position (x,y,z) of the domain. This is estimated in the 3D domain of the Augusta Bay by interpolating the experimental data collected by ICRAM during the oceanographic survey performed in the period 2005-2006 (Mare, 2008) (see section 1.2.2.2).

S1.3.4 Boundary conditions (lateral fluxes) - Dissolved methyl-mercury concentration

The Augusta basin can be considered as closed except for the inlets, rivers and sewerage (Valenti et al., 2017). Therefore, we fix the following lateral fluxes at boundaries of the domain:

$$\left[D_x \frac{\partial MeHg}{\partial x} - v_x MeHg\right] = \left[D_y \frac{\partial MeHg}{\partial y} - v_y MeHg\right] = 0, \tag{S41}$$

For all points of the basin where rivers and sewerage are localized, we set:

$$\left[D_x \frac{\partial MeHg}{\partial x} - v_x MeHg\right] = INPUT_{x_{point-source}} = \left(\frac{Q_{source}}{A_{source}}\right)\Big|_x \cdot MeHg_{source} \simeq 0, \tag{S42}$$

$$\left[D_y \frac{\partial MeHg}{\partial y} - v_y MeHg\right] = INPUT_{y_{point-source}} = \left(\frac{Q_{source}}{A_{source}}\right)\Big|_y \cdot MeHg_{source} \simeq 0, \tag{S43}$$

where

- Q_{source} is the average flow rate of water at the point source $[m^3/h]$;
- A_{source} is the longitudinal section of the point source $[m^2]$;
- $MeHg_{source}$ is the methyl-mercury concentration of the point source $[\mu g/m^3]$;
- $INPUT_{x_{point-source}}$ and $INPUT_{y_{point-source}}$ are the fluxes of mercury $[\mu g \cdot m^{-2} \cdot h^{-1}]$ along x-direction and y-direction, respectively, entering the basin from the point source.

The lateral fluxes of the methyl-mercury concentration at the inlets (Scirocco and Levante) of the basin (Salvagio Manta et al., 2016) (Sprovieri et al., 2011; Sprovieri, 2015; Salvagio Manta et al., 2016) as a function of depth and time are given by:

$$\begin{aligned}\phi^{MM}_{x_{inlet}}(z,t) &= \left[D_x \tfrac{\Delta MeHg}{\Delta x} - v_{x_{inlet}}(z,t) \cdot MeHg_{ext}(z)\right] = \\ &= \left[D_x \tfrac{\Delta MeHg}{\Delta x} + v_{x_{inlet}}(z,t) \cdot MeHg_{int}(z,t)\right]),\end{aligned} \tag{S44}$$

$$\begin{aligned}\phi^{MM}_{y_{inlet}}(z,t) &= \left[D_y \tfrac{\Delta MeHg}{\Delta y} - v_{y_{inlet}}(z,t) \cdot MeHg_{ext}(z)\right] = \\ &= \left[D_y \tfrac{\Delta MeHg}{\Delta y} + v_{y_{inlet}}(z,t) \cdot MeHg_{int}(z,t)\right]),\end{aligned} \tag{S45}$$

where

- $v_{x_{inlet}}(z,t)$ is the absolute value of the marine currents velocity at the inlet along the x-direction $[m/h]$;
- $v_{y_{inlet}}(z,t)$ is the absolute value of the marine currents velocity at the inlet along the y-direction $[m/h]$;
- $MeHg_{int}(z,t)$ ($MeHg_{ext}(z)$) is the internal (external) dissolved methyl-mercury concentrations close to the inlet $[\mu g/m^3]$;
- $\Delta MeHg$ is the difference between the internal and external dissolved methyl-mercury concentrations at the inlet of the basin $[\mu g/m^3]$;
- $\phi^{MM}_{x_{inlet}}(z,t)$ and $\phi^{MM}_{y_{inlet}}(z,t)$ are the horizontal fluxes of methyl-mercury concentration at the inlet $[\mu g \cdot m^{-2} \cdot h^{-1}]$.

The advection terms of Eqs. (S44)-(S45) are negative when the marine current velocities cause the external seawater to enter the Augusta Bay, while they are positive when the marine current velocities cause the internal seawater to come out from the basin. The annual net outflow of methyl-mercury from basin to open sea is obtained by integrating Eqs. (S44)-(S45) for the whole lateral surface of the two inlets and for the whole year.

In the same way, we obtain the annual net outflow of total mercury (O) from the basin towards the open sea by considering both the spatio-temporal behaviour of total mercury concentration reproduced by the advection-diffusion-reaction model, and the marine currents velocities at the inlets calculated by the SHYFEM model (see section 3).

S2 SPM concentration

The dynamics of the suspended particulate matter (SPM) concentration takes into account the physical processes investigated in the River model (Ciffroy, 2015; Melaku Canu et al., 2015; Neumeier et al., 2008; Ferrarin et al., 2008). The effects on the SPM dynamics are described by the following PDE:

$$\begin{aligned}\frac{\partial SPM}{\partial t} = \quad & +\frac{\partial}{\partial x}\left[D_x \frac{\partial SPM}{\partial x}\right] - \frac{\partial}{\partial x}(v_x \cdot SPM) + \frac{\partial}{\partial y}\left[D_y \frac{\partial SPM}{\partial y}\right] - \frac{\partial}{\partial y}(v_y \cdot SPM) \\ & +\frac{\partial}{\partial z}\left[D_z \frac{\partial SPM}{\partial z}\right] - \frac{\partial}{\partial z}(v_z \cdot SPM) - \frac{\partial}{\partial z}(w_s \cdot SPM) + S_L^{SPM},\end{aligned} \tag{S46}$$

where

- w_s is the settling velocity of particles $[m/h]$;
- S_L^{SPM} is the direct loads of suspended particulate matter $[\mu g/m^3]$.

Since the direct loads of SPM (Ciffroy, 2015; Melaku Canu et al., 2015) for the Augusta basin were unknown, the SPM concentration dynamics could not be reproduced correctly. Therefore, we reproduced the spatial distribution of SPM concentration at the steady state by interpolating the experimental data observed in recent samplings (October 2017) performed in the site investigated. From a mathematical point of view, the stationarity condition for the SPM concentration is described as follows:

$$\frac{\partial SPM}{\partial t} = 0. \tag{S47}$$

Moreover, we recall that the boundary conditions are not taken into account when the steady state condition is set.

The SPM values obtained in the sampling stations at the surface and bottom layers were linearly interpolated on the z-direction, in such a way to get different values for each vertical layer. Then, for each batimetry, on the x-y plane, the SPM value of each node of the grid has been determined as the weighted sum of the station values, with weight coefficients set as the inverse square distances of node centroids from the stations.

In general, the used setting is acceptable because the net flux of particles, due to the settling and the resuspension processes, is negligible according to a preliminary analysis performed by IAS-CNR (Oristano) (Neumeier et al., 2008; Ferrarin et al., 2008).

S2.1 SPM, SPIM and SPOM concentration

According to Zhang et al. (2014) and Melaku Canu et al. (2015) (Batrakova et al., 2014; Zhang et al., 2014; Melaku Canu et al., 2015), the suspended particulate matter is defined as follows:

$$SPM = SPIM + SPOM, \tag{S48}$$

where

- $SPIM$ is the Suspended Particulate Inorganic Matter concentration $[ng/l]$;
- $SPOM$ is the Suspended Particulate Organic Matter concentration $[ng/l]$.

Moreover, the particulate organic matter (POM) in dissolved-phase and the suspended particulate inorganic matter (SPIM) are given by:

$$POM = SPOM = f_{org} \cdot SPM, \tag{S49}$$

$$SPIM = (1 - f_{org}) \cdot SPM, \tag{S50}$$

where

- f_{org} is the organic fraction of suspended particulate matter in dissolved-phase $[dimensionless]$.

S3 The 3D hydrodynamic model

A three-dimensional, finite element hydrodynamic model, SHYFEM (Umgiesser et al., 2004) was adopted to reproduce the tide and wind induced water circulation, and the sediment transport processes in Augusta Harbor and adjacent coastal area. The model resolves, for each layer, the vertically integrated shallow water equations in their formulation with water levels and transport terms. It was applied with success to reproduce the main hydrodynamics in gulfs, harbors, lagoons and coastal seas (Cucco et al., 2012; Umgiesser et al., 2014; Ferrarin et al., 2014; Cucco et al., 2016a; Farina et al., 2018). The model uses finite elements for horizontal spatial discretizations, z-layers for vertical discretizations and a semi-implicit algorithm for integration in time. It accounts for barotropic, baroclinic and atmospheric pressure gradients as well as wind drag and bottom friction, non-linear advection and vertical turbulent processes. The solved equation system reads as:

$$\begin{gathered}
\frac{\partial U_l}{\partial t} + Adv_l^x - fV_l = gh_l \frac{\partial \zeta}{\partial x} - \frac{gh_l}{\rho_0} \frac{\partial}{\partial x} \int_{-H_l}^{\zeta} \rho' dz + \frac{h_l}{\rho_0} \frac{\partial p_a}{\partial x} + \frac{1}{\rho_0} \left(\tau_x^{top(l)} - \tau_x^{bot(l)} \right) + A_H \left(\frac{\partial^2 U_l}{\partial x^2} + \frac{\partial^2 U_l}{\partial y^2} \right), \\
\frac{\partial V_l}{\partial t} + Adv_l^y - fU_l = gh_l \frac{\partial \zeta}{\partial y} - \frac{gh_l}{\rho_0} \frac{\partial}{\partial y} \int_{-H_l}^{\zeta} \rho' dz + \frac{h_l}{\rho_0} \frac{\partial p_a}{\partial y} + \frac{1}{\rho_0} \left(\tau_y^{top(l)} - \tau_y^{bot(l)} \right) + A_H \left(\frac{\partial^2 V_l}{\partial x^2} + \frac{\partial^2 V_l}{\partial y^2} \right), \\
\frac{\partial \zeta}{\partial t} + \sum_l \frac{\partial U_l}{\partial x} + \sum_l \frac{\partial V_l}{\partial y},
\end{gathered} \tag{S51}$$

where l indicates the vertical layer, (U_l, V_l) the horizontal transport components in x- and y- directions for each layer l, Adv_l^x and Adv_l^y the advective terms for each layer l, p_a the atmospheric pressure, g the gravitational constant, f the Coriolis parameter, ζ the water level, ρ_0 the standard water density, ρ' the water density, h_l the layer thickness, H_l the depth of the bottom of the layer l, $\tau_x^{top(l)}$ and $\tau_x^{bot(l)}$ the stress terms in the x-direction at the top and bottom of each layer l, $\tau_y^{top(l)}$ and $\tau_y^{bot(l)}$ the stress terms in the y-direction at the top and bottom of each layer l, A_h the horizontal eddy viscosity. For the computation of the vertical diffusivities and viscosities, the General Ocean Turbulence Model (GOTM), described in Burchard and Petersen (1999) (Burchard and Petersen, 1999), was used. Wind and bottom friction terms, corresponding to the boundary conditions of the stress terms (τ_x,τ_y), are defined as:

$$\begin{aligned}
\tau_x^{surface} &= C_D \rho_a w_x \sqrt{w_x^2 + w_y^2}, \\
\tau_x^{bottom} &= C_B \rho_0 u_L \sqrt{u_L^2 + v_L^2}, \\
\tau_y^{surface} &= C_D \rho_a w_y \sqrt{w_x^2 + w_y^2}, \\
\tau_y^{bottom} &= C_B \rho_0 v_L \sqrt{u_L^2 + v_L^2},
\end{aligned} \tag{S52}$$

where C_D is the wind drag coefficient, C_B the bottom friction coefficient, ρ_a the air density, (w_x, w_y) the wind velocity components and (u_L, v_L) the bottom velocity components.

The hydrodynamic model is coupled with a sediment transport module that simulates the erosion, deposition and resuspension of both cohesive and non-cohesive sediments at the sea-bottom induced by the currents.

Specifically, as a first step, the sediment transport model computes the bed shear stress at the bottom boundary layer induced by the marine currents, to reproduce the re-suspension and the bed-load processes. Afterwards, the model calculates the suspended sediment concentration carried for advection and diffusion in the seawater. By this way, the rate of erosion and deposition are obtained for each nodes of the hydrodynamic finite element mesh.

The reader can refer to Umgiesser et al. (2004) (Umgiesser et al., 2004) and to Ferrarin et al. (2008) (Ferrarin et al., 2008) for a detailed description of the hydrodynamic and sediment transport model equations and adopted numerical methods.

S3.1 Model and simulations setup

The model domain was defined between the 15.05^o E and 15.55^o E and between the 36.95^o N and 37.35^o N, including the Augusta Harbor, the surrounding coastal areas and part of the Western Ionian Sea.

A finite element mesh composed by 21379 nodes and 40486 triangular elements with a spatial resolution varying between 20 meters for the inner harbor and few km for the far field was used for the horizontal discretization. The vertical direction was defined by 22 z-levels with layer depths ranging between 5 m and 200 m, by following an ad-hoc step distribution.

The data used to reproduce the model bathymetry were obtained integrating the large-scale GEBCO dataset (http://www.gebco.net) with data obtained from the digitalization of the nautical charts describing the Augusta Harbor and surrounding coastal areas. In Fig.5, the bathymetry and part of the finite element mesh reproducing the Augusta Bay and surrounding areas are shown.

The model was applied to reproduce the tide and wind induced water circulation, and the sediment transport during a ten years

period between January 2007 and December 2017. Baroclinic density gradients were neglected, being the interested coastal area not influenced by intense river inflows. The density vertical distribution was set as homogeneous and the GOTM (Burchard and Petersen, 1999) was used to reproduce the momentum transfer between each layers without any constrain related to the buoyancy variability along the vertical. The use of un-stratified model setup is generally acceptable if the interested domain is not affected by estuarine processes (Spydell et al., 2015; Cucco et al., 2016b). Therefore, wind and tide were set as the only external forcings promoting the water circulation in the harbor and surrounding coastal area. A similar approach was followed in several studies aimed at investigating the water circulation in bays, lagoons and harbors of the Mediterranean Sea, typically characterized by an extended shelf area and by the absence of intense fresh water inputs.

The wind data produced by the high-resolution non-hydrostatic meteorological prediction system SKIRON (Kallos and Pytharoulis, 2005) were used as model inputs. In particular, hourly fields of wind speeds and directions, obtained for the whole 10 years period and for the interested area with a spatial resolution of 0.008^o, were considered as model surface forcings. In addition, water elevation data were imposed along the model open boundary, corresponding to the open sea mesh border, following a Dirichlet condition. Adopted water level data consisted in hourly time series of tidal elevation. These data were obtained, for the whole considered period, from the global tidal model OTIS (http://volkov.oce.orst.edu/tides/otis.html). Common values of the main model parameters C_D and C_B (see Eq. (S52)) were imposed (Cucco et al., 2019) and a 10 years simulation run was carried out to reproduce the wind and tide induced water circulation inside the harbor at different vertical levels.

The sediments grain size variability at the sea bottom was reproduced using experimental data acquired during two previous samplings (May 2011 and June 2012). The grain sizes vary between 600 μm and 50 μm indicating a sea bottom constituted by sands, silt and very fine silt.

The model results consisted both in hourly fields of the horizontal components of the current velocities computed at the surface level, between 0 and 5 m, and at deeper layers, between 5 and 10 m, 10 and 20 m, and 20 and 30 m, and hourly datasets of eroded and deposed volumes of sediments for each nodes of the finite element mesh along the whole simulation run. These data were subsequently processed to be used as input data for the biogeochemical model. In particular, an interpolation procedure based on the Laplacian method was applied to regrid the SHYFEM model outputs (obtained on an unstructured mesh) on the biogeochemical model computational grid. In Fig.6, a snapshot of the horizontal components of the current velocities, obtained for the four selected vertical layers, are shown along with the points constituting the biogeochemical model computational regular mesh.

The results obtained from the interpolation procedure consist in hourly sequences of the horizontal components of the current speed and of the eroded/deposed volumes of sediments. These values were calculated, for a period of one year (from January 2011 to December 2011), at each point of the biogeochemical model grid and were used as input data to simulate the transport of the pollutants in the Augusta Bay.

S4 The advection-diffusion-reaction model for the eukaryotes population

Our study includes the analysis of the spatio-temporal behaviour of eukaryotes abundance, the most present planktonic population in the seawater of the Augusta Bay. In particular, we investigate the dynamics of the primary production of phytoplankton biomass by using an advection-diffusion-reaction model (Dutkiewicz et al., 2009; Morozov et al., 2010; Valenti et al., 2012; Denaro et al., 2013a, c, b; Valenti et al., 2015, 2016a, b, c, 2017), in which the effects of the growth limiting factors, i.e. light intensity and nutrient concentration, are taken into account. By solving the equations of the model, we get the steady spatial distribution of eukaryotes abundance, expressed in cells per unit volume and indicated by $b(x,y,z,t)$. Moreover, the spatial distributions of the phosphate concentration $R(x,y,z,t)$ and light intensity $I(x,y,z,t)$ are obtained.

The dynamics of the eukaryotes abundance is modeled by considering three processes (Valenti et al., 2012; Denaro et al., 2013a, c, b; Valenti et al., 2015, 2016a, b, c, 2017): i) net growth (reaction term); ii) passive movement (advection terms); iii) movement due to turbulence (diffusion terms).

The reaction term describes the nonlinear interactions between the net growth of eukaryotes abundance and the two limiting resources, i.e. light intensity and nutrient concentration. In particular, the net phytoplankton growth rate ($G(x,y,z,t)$) represents the balance between the gross production rate per capita and the mortality (Valenti et al., 2012; Denaro et al., 2013a, c, b; Valenti et al., 2015, 2016a, 2017). The former is given by $\min\{f_I(I), f_R(R)\}$, where $f_I(I)$ and $f_R(R)$ are obtained by the Michaelis-Menten formulas for light intensity and phosphate concentration (Valenti et al., 2012; Denaro et al., 2013a, c, b; Valenti et al., 2015, 2016a, 2017). The latter is described by the specific loss rate (m), in which we consider three processes: respiration, death, and grazing.

The advection terms allow to describe the effects on the spatial distribution of eukaryotes abundance induced both by the sinking velocity (w_z) along the z-direction, typical of the planktonic population investigated, and by the velocity field of marine currents reproduced by the SHYFEM model. The diffusion terms reproduce the effects of the turbulence on the spatial distribution of the eukaryotes population through the horizontal ($D_x = D_y$) and the vertical (D_v) turbulent diffusivities, whose values are the same used previously for mercury concentrations.

The equation for the dynamics of phosphate concentration $R(x,y,z,t)$ includes two reaction terms, which describe two different processes: i) the phosphate increase due to the recycling of the dead phytoplankton; ii) the phosphate decrease due to the uptake of the eukaryotes population. Moreover, also in this case, the effects of the local transport and turbulence, responsible for the mixing of nutrients in the 3D domain, are considered by inserting in the differential equation for the phosphate concentration three advection terms and three diffusion terms, respectively.

Finally, the light intensity $I(z,t)$ is assumed to decrease exponentially with the depth z, according to the Lambert-Beer's law (Valenti et al., 2012; Denaro et al., 2013a, c, b; Valenti et al., 2015, 2016a, 2017), and to vary as a function of time t due to the seasonal oscillations of the incident light intensity, $I_{in}(t)$.

Therefore, the model for eukaryotes population is defined by the following equations:

$$\begin{aligned}\frac{\partial b}{\partial t} = \; & +\frac{\partial}{\partial x}\left[D_x \frac{\partial b}{\partial x}\right] - \frac{\partial}{\partial x}(v_x b) + \frac{\partial}{\partial y}\left[D_y \frac{\partial b}{\partial y}\right] - \frac{\partial}{\partial y}(v_y b) + \frac{\partial}{\partial z}\left[D_z \frac{\partial b}{\partial z}\right] - \frac{\partial}{\partial z}(v_z b) - \frac{\partial}{\partial z}(w_z b) \\ & + b \cdot min\left(f_I(I), f_R(R)\right) - mb,\end{aligned} \tag{S53}$$

$$\begin{aligned}\frac{\partial R}{\partial t} = \; & +\frac{\partial}{\partial x}\left[D_x\frac{\partial R}{\partial x}\right]-\frac{\partial}{\partial x}(v_x R)+\frac{\partial}{\partial y}\left[D_y\frac{\partial R}{\partial y}\right]-\frac{\partial}{\partial y}(v_y R)+\frac{\partial}{\partial z}\left[D_z\frac{\partial R}{\partial z}\right]-\frac{\partial}{\partial z}(v_z R)+\textstyle\sum_i \varepsilon\cdot m\cdot\frac{b}{Y} \\ & -\tfrac{b}{Y}\cdot min\left(f_I(I),f_R(R)\right),\end{aligned} \tag{S54}$$

$$I(z,t) = I_{in}(t)\exp\left\{-\int_0^z \left[a_{bg}+a\cdot chl\,a\right]dZ\right\}. \tag{S55}$$

Here, m and w_z are the mortality and the sinking velocity of eukaryotes population, respectively; ε is the nutrient recycling coefficient for the eukaryotes population; $1/Y$ is the nutrient cell content of eukaryotes population; a_{bg} is the background turbidity; a is the average absorption coefficient for the eukaryotes population; $chl\,a$ is the *chlorophyll-a* concentration corresponding to the abundance of eukaryotes population. All parameters are set in accordance with the methods described in previous works (Hickman et al., 2010; Raven et al., 2005; Veldhuis et al., 2005; Timmermans et al., 2005), while the incident light intensity, $I_{in}(t)$, is obtained by using the remote sensing data. Finally, the *chlorophyll-a* concentration, $chl\,a$, is calculated by the theoretical results for the eukaryotes abundance by using the conversion curve obtained by Brunet et al. (Brunet et al., 2007).

The NP model is completed by a set of equations, which describe the nutrient and phytoplankton fluxes at the boundaries of Augusta Bay. Here, we set the following conditions for the eukaryotes abundance and the phosphate concentration: no biomass can enter or leave the area investigated except through the inlets; no nutrient flux is present through the water surface; the phosphate concentration at the deepest layer of the water column is fixed equal to the value measured previously close to Augusta Bay; no nutrient flux is present through the lateral surfaces except at the inlets; the eukaryotes abundance and the phosphate concentration are set constant out of the Augusta Bay (Mediterranean Sea); the lateral fluxes for eukaryotes population and phosphate concentration at the inlets depend on the behaviour of horizontal velocities. The boundary conditions for the eukaryotes abundance and the phosphate concentration are defined by the following equations:

$$\left[D_z\frac{\partial b}{\partial z}-(w_z+v_z)b_i\right]\Big|_{z=0} = \left[D_z\frac{\partial b}{\partial z}-(w_z+v_z)b\right]\Big|_{z=z_b} = 0, \tag{S56}$$

$$\left[D_x\frac{\partial b}{\partial x}-v_x b\right] = \left[D_y\frac{\partial b}{\partial y}-v_y b\right] = 0, \quad b(x_{inlet},y_{inlet},z) = b_{ext}, \tag{S57}$$

$$\frac{\partial R}{\partial z}\Big|_{z=0} = 0, \quad R(x,y,z_b) = R_{in}(x,y,z_b), \tag{S58}$$

$$\left[D_x\frac{\partial R}{\partial x}-v_x R\right] = \left[D_y\frac{\partial R}{\partial y}-v_y R\right] = 0, \quad R(x_{inlet},y_{inlet},z) = R_{ext}, \tag{S59}$$

where z_b is the depth of the water column in each position (x,y); b_{ext} is the average eukaryotes abundance in the Mediterranean Sea; $R_{in}(x,y,z_b)$ is the phosphate concentration kept constant at the deepest layer of the water column; R_{ext} is the average phosphate concentration in the Mediterranean Sea.

Eqs. (S53)-(S59) describe the three-dimensional advection-diffusion-reaction model used to reproduce the spatio-temporal behaviour of the eukaryotes abundance, the phosphate concentration and the light intensity in the seawater compartment of the Augusta Bay. The theoretical results obtained by this model are used to calculate the loads of dissolved mercury released by the particulate organic matter.

S5 The Phytoplankton MERLIN-Expo model for the mercury contents in the eukaryotes population

The dynamics of the mercury content in the eukaryotes population is analyzed in the Augusta Bay by using the Phytoplankton MERLIN-Expo model (Radomyski and Ciffroy, 2015). Specifically, we investigate the behaviour of the most abundant two mercury species within the phytoplankton cells, i.e. inorganic mercury and methyl-mercury. By solving the equations of the model, we obtain the dynamics of the amount of inorganic mercury and methyl-mercury present in each eukaryotes cell, indicated by $PHg^{II}(x,y,z,t)$ and $PMeHg(x,y,z,t)$, respectively.

The dynamics of the content of inorganic mercury and methyl-mercury in each eukaryotes cell is modeled by considering three processes (Radomyski and Ciffroy, 2015): i) mercury absorption through the cell wall; ii) mercury elimination (excretion) through the cell wall; iii) mercury elimination via dilution. The first process is described by the uptake rate constant for the mercury, which is obtained by the water layer diffusion resistance, the lipid permeation resistance and the mercury concentration in the seawater. The second process is described by the elimination rate constant for the mercury, which depends on the water layer diffusion resistance, the lipid permeation resistance and the water-dissolved organic carbon partition coefficient. The third process is described by the growth rate constant for the eukaryotes, which is obtained by the phytoplankton growth rate and the phytoplankton weight.

Thus, the Phytoplankton Merlin-Expo model (Radomyski and Ciffroy, 2015) for the two mercury species embedded at the eukaryotes cells is defined by the following equations:

$$\frac{dPHg^{II}}{dt} = W_{phy} \cdot k_{phy,up,inor} \cdot Hg^{II} - PHg^{II} \cdot (k_{phy,exc,inor} + k_{phy,gro}), \tag{S60}$$

$$\frac{dPMeHg}{dt} = W_{phy} \cdot k_{phy,up,meth} \cdot MeHg - PMeHg \cdot (k_{phy,exc,meth} + k_{phy,gro}), \tag{S61}$$

where W_{phy} is the phytoplankton cell weight, $k_{phy,up,inor}$ is the inorganic mercury uptake rate constant, $k_{phy,up,meth}$ is the methyl-mercury uptake rate constant, $k_{phy,exc,inor}$ is the elimination rate constant for the inorganic mercury, $k_{phy,exc,meth}$ is the elimination rate constant for the methyl-mercury; $k_{phy,gro}$ is the growth rate constant. According to the Phytoplankton Merlin-Expo model (Radomyski and Ciffroy, 2015), the rates of Eqs. (S60)-(S61) are calculated as follows:

$$k_{phy,up,inor} = \frac{W_{phy}^{-k}}{\rho_{water} + \rho_{lipid} \cdot (Hg^{II})^{b_{lipid}}}, \tag{S62}$$

$$k_{phy,up,meth} = \frac{W_{phy}^{-k}}{\rho_{water} + \rho_{lipid} \cdot (MeHg)^{b_{lipid}}}, \tag{S63}$$

$$k_{phy,exc,inor} = \frac{W_{phy}^{-k}}{\rho_{water} + \rho_{lipid}} \cdot \frac{1}{p_{carbonphy} \cdot 10^{log_{10} K_d^{II}}}, \tag{S64}$$

$$k_{phy,exc,meth} = \frac{W_{phy}^{-k}}{\rho_{water} + \rho_{lipid}} \cdot \frac{1}{p_{carbonphy} \cdot 10^{log_{10} K_d^{MM}}}, \tag{S65}$$

$$k_{phy,gro} = a_{growth} \cdot V_{cell}^{-b_{growth}}, \tag{S66}$$

where W_{phy} and V_{cell} are the phytoplankton weight and the phytoplankton cell volume of the eukaryotes, respectively; k is the allometric rate exponent of the phytoplankton; ρ_{lipid} and ρ_{water} are the lipid layer permeation resistance and the water layer diffusion resistance for the uptake of chemicals from water, respectively; b_{lipid} is the lipid permeation resistance exponent; Hg^{II} and $MeHg$ are the inorganic mercury concentration and the methyl-mercury concentration in the seawater, respectively; $p_{carbonphy}$ is the organic carbon fraction of phytoplankton; $log_{10} K_d^{II}$ and $log_{10} K_d^{MM}$ are the water-dissolved organic carbon partition coefficients for the inorganic mercury and the methyl-mercury, respectively; a_{growth} and b_{growth} are the intercept and the slope of the phytoplankton growth rate, respectively. The eukaryotes weight, W_{phy}, and the phytoplankton cell volume, V_{cell}, are estimated by using the experimental findings reported in previous works (Radomyski and Ciffroy, 2015; Pickhardt and Fischer, 2007; Strickland, 1960). The mercury concentrations, Hg^{II} and $MeHg$, in the seawater are obtained by the advection-diffusion-reaction model (see section 1). All other parameters are set at the same values given in "The Phytoplankton Merlin-Expo model" (Radomyski and Ciffroy, 2015; Hendricks, 2007; Hauck et al., 2011; Allison and Allison, 2005).

As initial conditions, we fix that the mercury contents in each eukaryotes cell depend on both the dissolved mercury concentrations in marine environment and the volume concentration factors estimated for specific chemicals (inorganic mercury and methyl-mercury) and phytoplankton species (eukaryotes) (Pickhardt and Fischer, 2007). In particular, the inorganic mercury content and the methyl-mercury content at the initial time ($t = 0$) are given by:

$$PHg^{II}(0) = W_{phy} \cdot VCF^{II} \cdot Hg^{II}(0), \qquad PMeHg(0) = W_{phy} \cdot VCF^{MM} \cdot MeHg(0) \tag{S67}$$

where VCF^{II} and VCF^{MM} are the volume concentration factors for the inorganic mercury and the methyl-mercury, respectively, in the eukaryotes; $Hg^{II}(0)$ and $MeHg(0)$ are the inorganic mercury concentration and the methyl-mercury concentration at the initial time $t = 0$.

Eqs. (S60)-(S66) constitute the Phytoplankton MERLIN-Expo model used to reproduce the dynamics of the mercury contents within the eukaryotes cells, which populate the Augusta Bay. The theoretical results obtained by this model are used to calculate the loads of dissolved mercury released by the particulate organic matter.

References

Allison, J. D. and Allison, T. L.: Partition coefficients for metals in surface water, soil, and waste, U.S. Environmental Protection Agency, Washington, DC, 2005.

Bagnato, E., Sprovieri, M., Barra, M., Bitetto, M., Bonsignore, M., Calabrese, S., Di Stefano, V., Oliveri, E., Parello, F., and Mazzola, S.: The sea-air exchange of mercury (Hg) in the marine boundary layer of the Augusta basin (southern Italy): Concentrations and evasion flux, Chemosphere, 93, 2024–2032, https://doi.org/10.1016/j.chemosphere.2013.07.025, 2013.

Batrakova, N., Travnikov, O., and Rozovskaya, O.: Chemical and physical transformations of mercury in the ocean: a review, Ocean Sci., 10, 1047–1063, https://doi.org/https://doi.org/10.5194/os-10-1047-2014, 2014.

Brunet, C., Casotti, R., Vantrepotte, V., and Conversano, F.: Vertical variability and diel dynamics of picophytoplankton in the Strait of Sicily, Mediterranean Sea, in summer, Mar. Ecol. Prog. Ser., 346, 15–26, 2007.

Burchard, H. and Petersen, O.: Models of turbulence in the marine environment. A comparative study of two-equation turbulence models, J. Mar. Syst., 21(1-4), 23–53, https://doi.org/10.1016/S0924-7963(99)00004-4, 1999.

Ciffroy, P.: The River MERLIN-Expo model, Fun Project 4 - Seventh Framework Programme, 2015.

Cossa, D. and Coquery, M.: The Handbook of Environmental Chemistry, Vol. 5, Part K (2005): 177-208. The Mediterranean Mercury Anomaly, a Geochemical or a Biologocal Issue, Springer-Verlag Berlin Heidelberg, 2005.

Covelli, S., Faganeli, J., De Vittor, C., Predonzani, S., Acquavita, A., and Horvat, M.: Benthic fluxes of mercury species in a lagoon environment (Grado Lagoon, Northern Adriatic Sea, Italy), Appl. Geochem., 23, 529–546, https://doi.org/10.1016/j.apgeochem.2007.12.011, 2008.

Cucco, A., Sinerchia, M., Lefrançois, C., Magni, P., Ghezzo, M., Umgiesser, G., Perilli, A., and Domenici, P.: A metabolic scope based model of fish response to environmental changes, Ecol. Model., 237-238, 132–141, https://doi.org/10.1016/j.ecolmodel.2012.04.019, 2012.

Cucco, A., Quattrocchi, G., Olita, A., Fazioli, L., Ribotti, A., Sinerchia, M., Tedesco, C., and Sorgente, R.: Hydrodynamic modeling of coastal seas: the role of tidal dynamics in the Messina Strait, Western Mediterranean Sea, Nat. Hazard Earth Sys., 16, 1553–1569, https://doi.org/10.5194/nhess-16-1553-2016, 2016a.

Cucco, A., Quattrocchi, G., Satta, A., Antognarelli, F., De Biasio, F., Cadau, E., Umgiesser, G., and Zecchetto, S.: Predictability of wind-induced sea surface transport in coastal areas, J. Geophys. Res. Oceans, 121(8), 5847–5871, https://doi.org/https://doi.org/10.1002/2016JC011643, 2016b.

Cucco, A., Quattrocchi, G., and Zecchetto, S.: The role of temporal resolution in modeling the wind induced sea surface transport in coastal seas, J. Mar. Syst., 193, 46–58, https://doi.org/https://doi.org/10.1016/j.jmarsys.2019.01.004, 2019.

Denaro, G., Valenti, D., La Cognata, A., Spagnolo, B., Bonanno, A., Basilone, G., Mazzola, S., Zgozi, S., Aronica, S., and Brunet, C.: Spatio-temporal behaviour of the deep chlorophyll maximum in Mediterranean Sea: Development of a stochastic model for picophytoplankton dynamics, Ecol. Complex., 13, 21–34, https://doi.org/10.1016/j.ecocom.2012.10.002, 2013a.

Denaro, G., Valenti, D., Spagnolo, B., Basilone, G., Mazzola, S., Zgozi, S., Aronica, S., and Bonanno, A.: Dynamics of two picophytoplankton groups in Mediterranean Sea: Analysis of the Deep Chlorophyll Maximum by a stochastic advection-reaction-diffusion model, PLoS ONE, 8(6), e66 765, https://doi.org/10.1371/journal.pone.0066765, 2013b.

Denaro, G., Valenti, D., Spagnolo, B., Bonanno, A., Basilone, G., Mazzola, S., Zgozi, S., and Aronica, S.: Stochastic dynamics of two picophytoplankton populations in a real marine ecosystem, Acta Phys. Pol. B, 44, 977–990, https://doi.org/10.5506/APhysPolB.44.977, 2013c.

Denman, K. L. and Gargett, A. E.: Time and space scales of vertical mixing and advection of phytoplankton in the upper ocean, Limnol. Oceanogr., 28, 801–815, https://doi.org/https://doi.org/10.4319/lo.1983.28.5.0801, 1983.

D'Ortenzio, F.: Space and time occurrence of algal blooms in the Mediterranean: their significance for the trophic regime of the basin, PhD Thesis, Open University of London, UK, 2003.

Driscoll, C. T., Mason, R. P., Chan, H. M., Jacob, D. J., and Pirrone, N.: Mercury as a Global Pollutant: Sources, Pathways, and Effects, Environ. Sci. Technol., 47, 4967–4983, https://doi.org/10.1021/es305071v, 2013.

Dutkiewicz, S., Follows, M. J., and Bragg, J. G.: Modeling the coupling of ocean ecology and biogeochemistry., Global Biogeochem. Cycles, p. GB4017, https://doi.org/https://doi.org/10.1029/2008GB003405, 2009.

Farina, S., Quattrocchi, G., Guala, I., and Cucco, A.: Hydrodynamic patterns favouring sea urchin recruitment in coastal areas: A Mediterranean study case, Mar. Environ. Res., 139, 182–192, https://doi.org/10.1016/j.marenvres.2018.05.013, 2018.

Ferrarin, C., Umgiesser, G., Cucco, A., Hsu, T. W., Roland, A., and Amos, C. L.: Development and validation of a finite element morphological model for shallow water basins, Coast. Eng., 55, 716–731, https://doi.org/10.1016/j.coastaleng.2008.02.016, 2008.

Ferrarin, C., Bajo, M., Bellafiore, D., Cucco, A., De Pascalis, F., and Ghezzo, M.: Toward homogenization of Mediterranean lagoons and their loss of hydrodiversity, Geophys. Res. Lett., 41(16), 5935–5941, https://doi.org/https://doi.org/10.1002/2014GL060843, 2014.

Han, S., Lehman, R. D., Choe, K. Y., and Gill, A.: Chemical and physical speciation of mercury in Offatts Bayou: A seasonally anoxic bayou in Galveston Bay, Limnol. Oceanogr., 52(4), 1380–1392, https://doi.org/https://doi.org/10.4319/lo.2007.52.4.1380, 2007.

Hauck, A. J., Hendricks, H. W. M., Huijbregts, M. A. J., Ragas, A. M. J., Van der Meent, D., and Hendricks, A. J.: Parameter uncertainty in modeling bioaccumulation factors of fish, Environ. Toxicol. Chem., 30(2), 403–412, https://doi.org/10.1002/etc.393, 2011.

Hendricks, A. J.: The power of size: A meta-analysis reveals consistency of allometric regressions, Ecol. Model., 205, 196–208, https://doi.org/10.1016/j.ecolmodel.2007.02.029, 2007.

Hickman, A., Dutkiewicz, S., Williams, R., and Follows, M.: Modelling the effects of chromatic adaptation on phytoplankton community structure in the oligotrophic ocean, Mar. Ecol. Prog. Ser., 406, 1–17, 2010.

Hines, M. E., Potrait, E. N., Covelli, S., Faganeli, J., Emili, A., Zizek, E., and Horvat, M.: Mercury methylation and demethylation in Hg-contaminated lagoon sediments (Marano and Grado Lagoon, Italy), Estuar. Coast. Shelf Sci., 113, 85–95, https://doi.org/10.1016/j.ecss.2011.12.021, 2012.

Horvat, M., Kotnik, J., Logar, M., Fajon, V., Zvoranic, T., and Pirrone, N.: Speciation of mercury in surface and deep-sea waters in the Mediterranean Sea, Atmospheric Environ., 37(1), S93–S108, https://doi.org/10.1016/S1352-2310(03)00249-8, 2003.

Kallos, G. and Pytharoulis, I.: Short-term predictions (weather forecasting purposes), Encyclopedia of Hydrological Sciences, edited by M. G. Anderson, pp. 2791-2811, John Wiley, London, U.K., 2005.

Katz, E. J., Bruce, J. G., and Petrie, B. D.: Salt and mass flux in the Atlantic Equatorial Undercurrent, Deep-Sea Res., 26, 139–160, 1979.

Liu, G., Cai, J., and O'Driscoll, N.: Environmental Chemistry and Toxycology of Mercury, John Wiley and Sons, Inc., Hoboken, New Jersey, 2012.

Mare, I. I. C. P. L. R. S. E. T. A. A.: Progetto preliminare di bonifica dei fondali della rada di Augusta nel sito di interesse nazionale di Priolo e Elaborazione definitiva, BoI-Pr-SI-PR-Rada di Augusta-03.22, 2008.

Massel, S. R.: Fluid Mechanics for Marine Ecologists, Springer-Verlag, Berlin Heidelberg, 1999.

Melaku Canu, D., Rosati, G., Solidoro, C., Heimbürger, L., and Acquavita, A.: A comprehensive assessment of the mercury budget in the Marano-Grado Lagoon (Adriatic Sea) using a combined observational modeling approach, Mar. Chem., 177, 742–752, https://doi.org/10.1016/j.marchem.2015.10.013, 2015.

Monperrus, M., Tessier, E., Amouroux, D., Leynaert, A., Huonnic, P., and Donard, O. F. X.: Mercury methylation, demethylation and reduction rates in coastal and marine surface waters of the Mediterranean Sea, Mar. Chem., 107, 49–63, https://doi.org/10.1016/j.marchem.2007.01.018, 2007a.

Monperrus, M., Tessier, E., Point, D., Vidimova, K., Amouroux, D., Guyoneaud, R., Leynaert, A., Grall, J., Chauvaud, L., Thouzeau, G., and Donard, O. F. X.: The biogeochemistry of mercury at the sediment-water interface in the Thau Lagoon. 2. Evaluation of mercury methylation potential in both surface sediment and the column, Estuar. Coast. Shelf Sci., 72, 485–486, https://doi.org/https://doi.org/10.1016/j.ecss.2006.11.014, 2007b.

Morozov, A., Arashkevich, E., Nikishina, A., and Solovyev, K.: Nutrient-rich plankton communities stabilized via predator-prey interactions: revisiting the role of vertical heterogeneity, Math. Med. Biol., 28(2), 185–215, https://doi.org/10.1093/imammb/dqq010, 2010.

Neumeier, U., Ferrarin, C., Amos, C. L., Umgiesser, G., and Li, M. Z.: Sedtrans05: An improved sediment-transport model for continental shelves and coastal waters with a new algorithm for cohesive sediments, Comput. Geosci., 34, 1223–1242, https://doi.org/10.1016/j.cageo.2008.02.007, 2008.

Oliveri, E., Manta, D. S., Bonsignore, M., Cappello, S., Tranchida, G., Bagnato, E., Sabatino, N., Santisi, S., and Sprovieri, M.: Mobility of mercury in contaminated marine sediments: Biogeochemical pathways, Mar. Chem., 186, 1–10, https://doi.org/10.1016/j.marchem.2016.07.002, 2016.

Pacanowski, R. and Philander, S. G. H.: Parameterization of Vertical Mixing in Numerical Models of Tropical Oceans, J. Phys. Oceanogr., 11, 1443–1451, https://doi.org/10.1175/1520-0485(1981)011$<$ 1443 : $POVMIN >$2.0.CO;2, 1981.

Peters, H., Gregg, M. C., and Toole, J. M.: On the Parameterization of Equatorial Turbulence, J. Geophys. Res., 93, 1199–1218, https://doi.org/https://doi.org/10.1029/JC093iC02p01199, 1988.

Pickhardt, P. C. and Fischer, N. S.: Accumulation of Inorganic and Methylmercury by Freshwater Phytoplankton in Two Contrasting Water Bodies, Environ. Sci. Technol., 41, 125–131, https://doi.org/10.1021/es060966w, 2007.

Qureshi, A., O'Driscoll, N. J., MacLeod, M., Neuhold, Y. M., and Hungerbuhler, K.: Photoreactions of mercury in surface ocean water: gross reaction kinetics and possible pathways, Environ. Sci. Technol., 44, 644–649, https://doi.org/10.1021/es9012728, 2010.

Radomyski, A. and Ciffroy, P.: The Phytoplankton MERLIN-Expo model, Fun Project 4 - Seventh Framework Programme, 2015.

Raven, J. A., Finkel, Z. V., and Irwin, A. J.: Picophytoplankton: bottom-up an top-down controls on ecology and evolution, J. Geophys. Res., 55, 209–215, 2005.

Salvagio Manta, D., Bonsignore, M., Oliveri, E., Barra, M., Tranchida, G., Giaramita, L., Mazzola, S., and Sprovieri, M.: Fluxes and the mass balance of mercury in Augusta Bay (Sicily, southern Italy), Estuar. Coast. Shelf Sci., 181, 134–143, https://doi.org/10.1016/j.ecss.2016.08.013, 2016.

Schulz, H. D. and Zabel, M.: Marine Geochemistry, Springer - Verlag Berlin Heidelberg, 2006.

Soerensen, A. L., Sunderland, E. M., Holmes, C. D., Jacob, D. J., Yantosca, R. M., Skov, H., Christensen, J. H., Strode, S. A., and Mason, R. P.: An improved global model for air-sea exchange of mercury: High concentrations over the north Atlantic, Environ. Sci. Technol., 44, 8574–8580, https://doi.org/10.1021/es102032g, 2010.

Sørensen, P. B., Fauser, P., Carlsen, L., and Vikelsøe, J.: Theoretical evaluation of the sediment/water exchange description in generic compartment models (SimpleBox), NERI Technical Report No.360, 2001.

Sprovieri, M.: Inquinamento ambientale e salute umana, il caso studio della Rada di Augusta, CNR Edizioni, P. Aldo Moro, 7, I-00185 Roma, Italia, 2015.

Sprovieri, M., Oliveri, E., Di Leonardo, R., Romano, E., Ausili, A., Gabellini, M., Barra, M., Tranchida, G., Bellanca, A., Neri, R., Budillon, F., Saggiomo, R., Mazzola, S., and Saggiomo, V.: The key role played by the Augusta basin (southern Italy) in the mercury contamination of the Mediterranean Sea, J. Environ. Monit., 13, 1753–1760, https://doi.org/10.1039/C0EM00793E, 2011.

Spydell, M. S., Feddersen, F., Olabarrieta, M., Chen, J., Guza, R. T., Raubenheimer, B., and Elgar, S.: Observed and modeled drifters at a tidal inlet, J. Geophys. Res. Oceans, 120, 4825–4844, https://doi.org/10.1002/2014JC010541, 2015.

Strickland, J. D. H.: Measuring the Production of Marine Phytoplankton, Fisheries Research Board of Canada (Bulletin), 1960.

Strode, S. A., Jaegle, L., Selin, N., Jacob, D. J., Park, R., Yantosca, R. M., Mason, R. P., and Slemr, F.: Air-sea exchange in the global mercury cycle, Global Biogeochem. Cy., 21, GB1017, https://doi.org/https://doi.org/10.1029/2006GB002766, 2007.

Sunderland, E. M., Gobas, F. A. P. C., Branfireum, B. A., and Heyes, A.: Environmental controls on the speciation and distribtuion of mercury in coastal sediments, Mar. Chem., 102, 111–123, https://doi.org/10.1016/j.marchem.2005.09.019, 2006.

Thi, N. N. P., Huisman, J., and Sommeijer, B. P.: Simulation of three-dimensional phytoplankton dynamics: competition in light-limited environments, J. Comput. Appl. Math., 174, 57–77, https://doi.org/10.1016/j.cam.2004.03.023, 2005.

Timmermans, K. R., van der Wagt, B., Veldhuis, M. J. W., Maatman, A., and de Baar, H. J. W.: Physiological responses of three species of marine pico-phytoplankton to ammonium, phospahte, iron and light limitation, J. Sea Res., 53, 109–120, 2005.

Tveito, A. and Winther, R.: Introduction to Partial Differential Equations: A Computational Approach, Springer-Verlag, New York, 1998.

Umgiesser, G.: SHYFEM. Finite Element Model for Coastal Seas. User Manual, The SHYFEM Group, Georg Umgiesser, ISMAR-CNR, Venezia, Italy, 2009.

Umgiesser, G., Canu, D. M., Cucco, A., and Solidoro, C.: A finite element model for the Venice Lagoon. Development, set up, calibration and validation, J. Mar. Syst., 51, 123–145, https://doi.org/10.1016/j.jmarsys.2004.05.009, 2004.

Umgiesser, G., Ferrarin, C., Cucco, A., De Pascalis, F., Bellafiore, D., Ghezzo, M., and Bajo, M.: Comparative hydrodynamics of 10 Mediterranean lagoons by means of numerical modeling, J. Geophys. Res. Oceans, 119(4), 2212–2226, https://doi.org/https://doi.org/10.1002/2013JC009512, 2014.

Valenti, D., Denaro, G., La Cognata, A., Spagnolo, B., Bonanno, A., Mazzola, S., Zgozi, S., and Aronica, S.: Picophytoplankton dynamics in noisy marine environment, Acta Phys. Pol. B, 43, 1227–1240, https://doi.org/10.5506/APhysPolB.43.1227, 2012.

Valenti, D., Denaro, G., Spagnolo, B., Conversano, F., and Brunet, C.: How diffusivity, thermocline and incident light intensity modulate the dynamics of deep chlorphyll maximum in Tyrrhenian Sea, PLoS ONE, 10(1), e0115 468, https://doi.org/https://doi.org/10.1371/journal.pone.0115468, 2015.

Valenti, D., Denaro, G., Conversano, F., Brunet, C., Bonanno, A., Basilone, G., Mazzola, S., and Spagnolo, B.: The role of noise on the steady state distributions of phytoplankton populations, J. Stat. Mech., p. 054044, https://doi.org/10.1088/1742-5468/2016/05/054044, 2016a.

Valenti, D., Denaro, G., Spagnolo, B., Mazzola, S., Basilone, G., Conversano, F., Brunet, C., and Bonanno, A.: Stochastic models for phytoplankton dynamics in Mediterranean Sea, Ecol. Complex., 27, 84–103, https://doi.org/10.1016/j.ecocom.2015.06.001, 2016b.

Valenti, D., Giuffrida, A., Denaro, G., Pizzolato, N., Curcio, L., Mazzola, S., Basilone, G., Bonanno, A., and Spagnolo, B.: Noise Induced Phenomena in the Dynamics of Two Competing Species, Math. Model. Nat. Phenom., 11(5), 158–174, https://doi.org/https://doi.org/10.1051/mmnp/201611510, 2016c.

Valenti, D., Denaro, G., Ferreri, R., Genovese, S., Aronica, S., Mazzola, S., Bonanno, A., Basilone, G., and Spagnolo, B.: Spatio-temporal dynamics of a planktonic system and chlorophyll distribution in a 2D spatial domain: matching model and data, Sci. Rep., 7, 220, https://doi.org/https://doi.org/10.1051/mmnp/201611510, 2017.

Veldhuis, M. J. W., Timmermans, K. R., Croot, P., and Van Der Wagt, B.: Picophytoplankton; a comparative study of their biochemical composition and photosynthetic properties, J. Sea Res., 53, 7–24, 2005.

Whalin, L., Kim, E., and Mason, R.: Factors influencing the oxidation, reduction, methylation and demethylation of mercury species in coastal waters, Mar. Chem., 107, 278–294, https://doi.org/10.1016/j.marchem.2007.04.002, 2007.

Zhang, Y., Jaeglé, L., and Thompson, L.: Natural biogeochemical cycle of mercury in a global three-dimensional ocean tracer model, Global Biogeochem. Cy., 28, GB004 814, https://doi.org/10.1002/2014GB004814, 2014.

SUPPLEMENTARY FIGURES AND TABLES

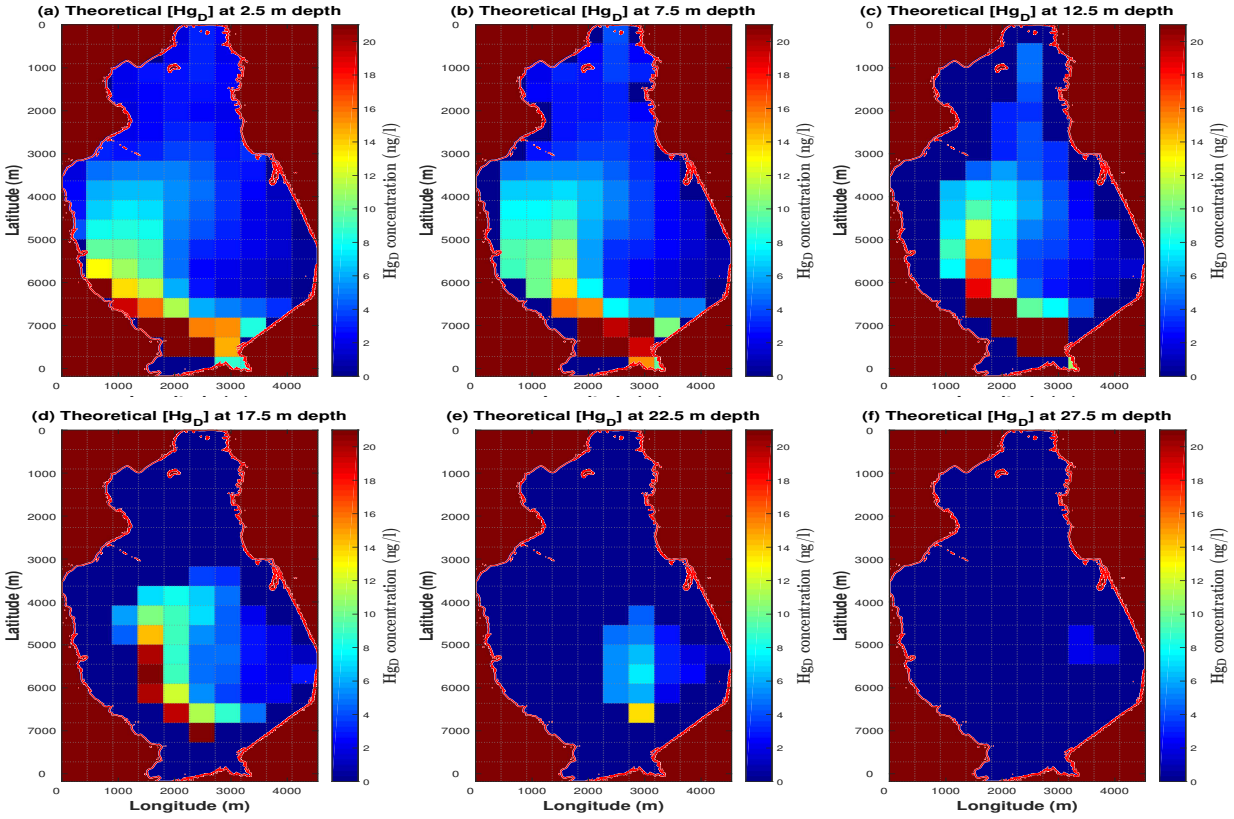

Figure S1. Theoretical distributions of the dissolved mercury concentration obtained by the model for the six different depths of the seawater compartment. The maps reproduce the spatial behaviour of the dissolved mercury concentration at the depths 2.5 m (panel a), 7.5 m (panel b), 12.5 m (panel c), 17.5 m (panel d), 22.5 m (panel e) and 27.5 m (panel f) during the sampling period of May 2011.

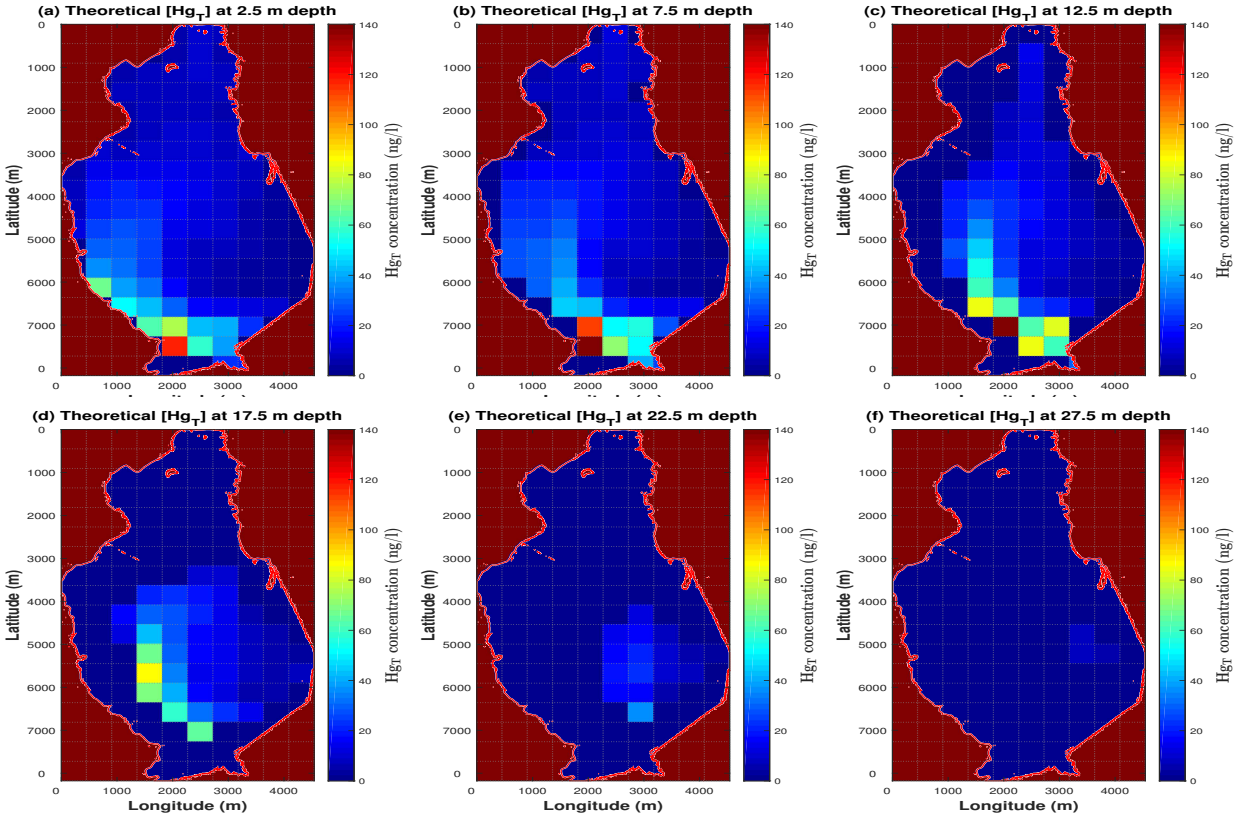

Figure S2. Theoretical distributions of the total mercury concentration obtained by the model for the six different depths of the seawater compartment. The maps reproduce the spatial behaviour of the total mercury concentration at the depths 2.5 m (panel a), 7.5 m (panel b), 12.5 m (panel c), 17.5 m (panel d), 22.5 m (panel e) and 27.5 m (panel f) during the sampling period of May 2011.

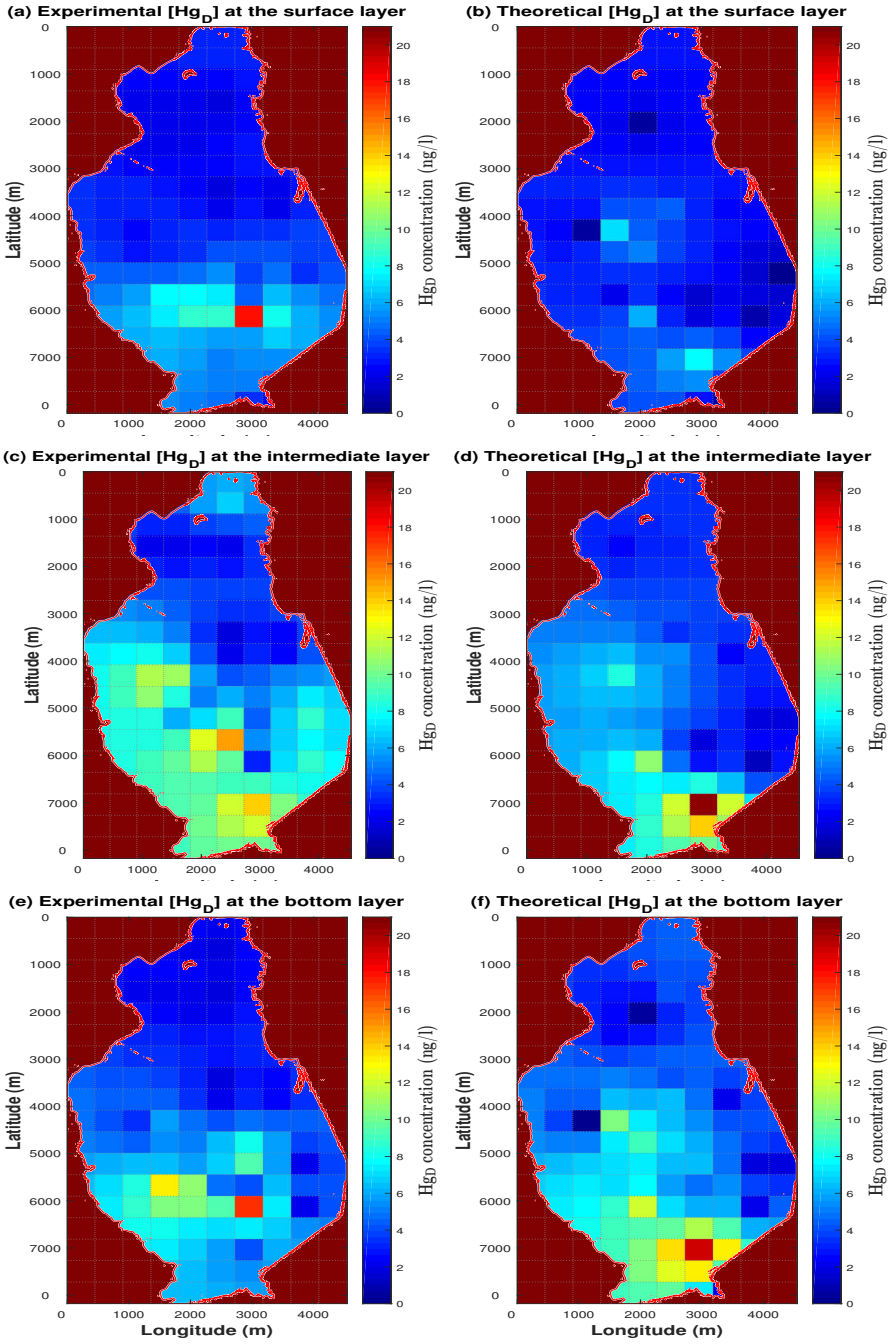

Figure S3. Comparison between the experimental data and the theoretical results for the dissolved mercury concentration. The maps reproduce the spatial distributions of the dissolved mercury concentration at surface layer (panels a, b), intermediate layer (panels c,d) and bottom layer (panels e,f) of the water column during the sampling period of May 2011. The spatial distributions are obtained by interpolating the experimental data collected in the Augusta Bay, and the theoretical results calculated by the model.

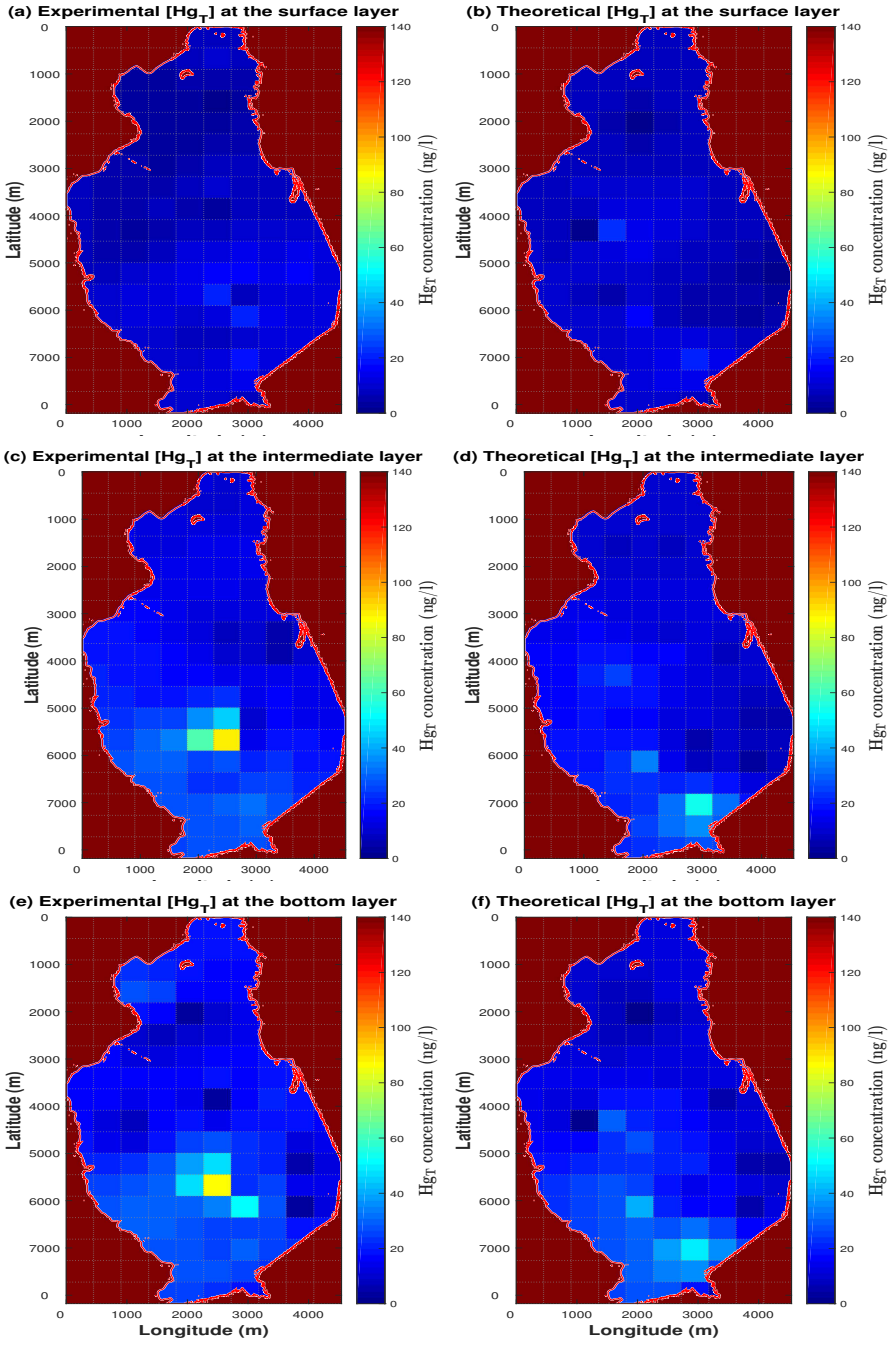

Figure S4. Comparison between the experimental data and the theoretical results for the total mercury concentration. The maps reproduce the spatial distributions of the total mercury concentration at surface layer (panels a, b), intermediate layer (panels c,d) and bottom layer (panels e,f) of the water column during the sampling period of May 2011. The spatial distributions are obtained by interpolating the experimental data collected in the Augusta Bay, and the theoretical results calculated by the model.

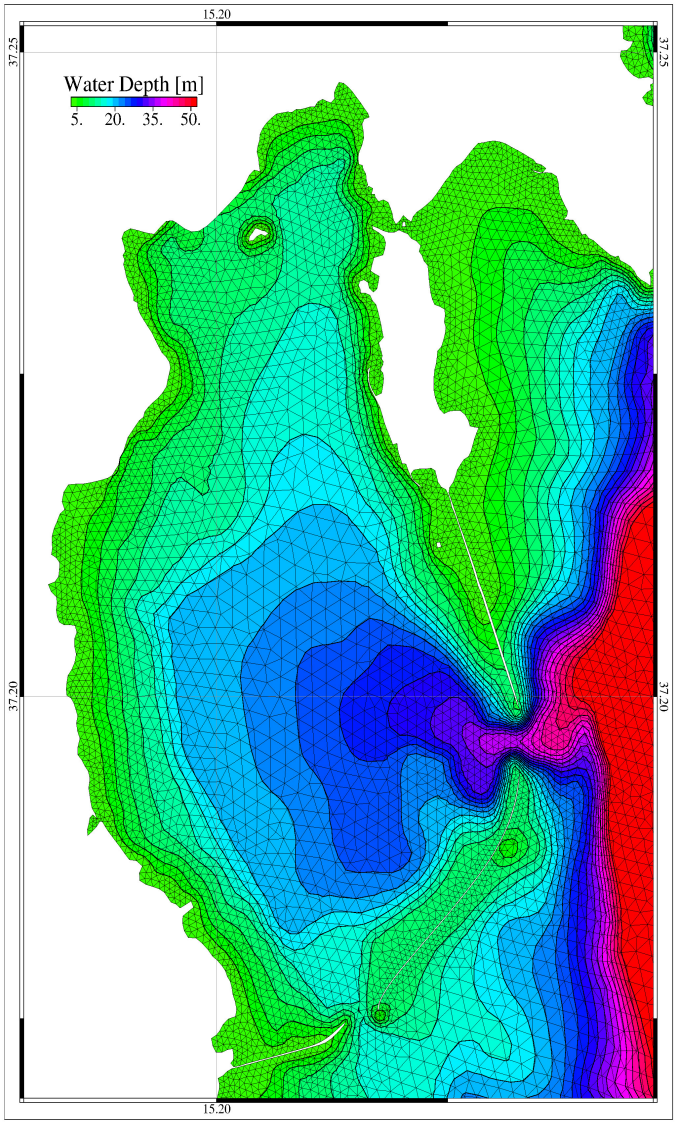

Figure S5. Zoom of the finite element mesh and bathymetry for the Augusta Bay and surrounding coastal area.

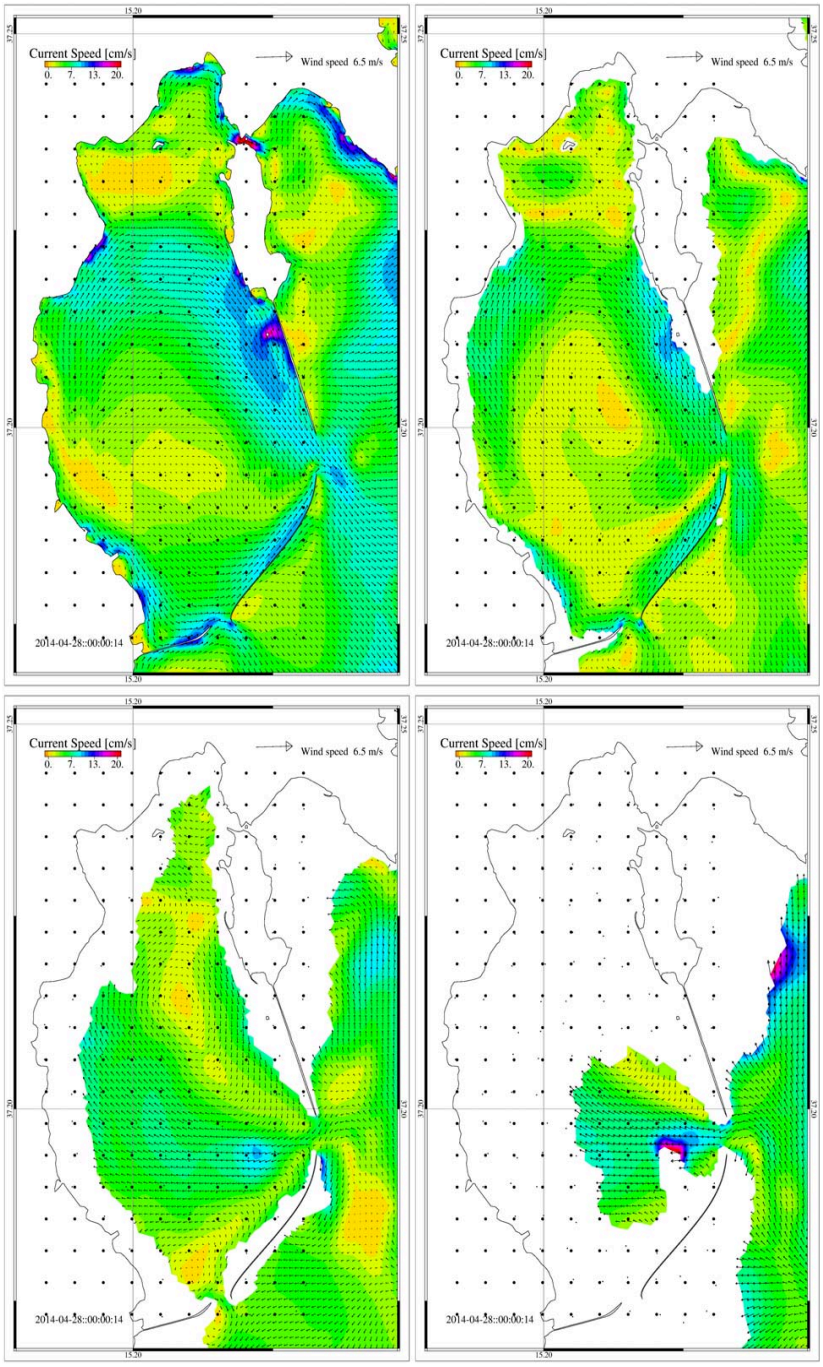

Figure S6. Velocity fields of marine currents computed by SHYFEM at different vertical levels in the Augusta harbour area. Black dots indicate the mesh points of the biogeochemical model domain. From left to right, the maps reproduce results obtained for the layers between 0-5 m, 5-10 m, 10-20 m e 20-30 m, respectively.

Symbol	Interpretation	Unit	Value	Reference
D_x	Horizontal turbulent diffusivity along x-axis	$m^2\ h^{-1}$	3600.0	Massel (1999)
D_y	Horizontal turbulent diffusivity along y-axis	$m^2\ h^{-1}$	3600.0	Massel (1999)
D_z	Vertical turbulent diffusivity along z-axis	$m^2\ h^{-1}$	3.6	Pham Thi at al. (2005)
v_z	Vertical component of velocity field	$m\ h^{-1}$	0.0	Experimental data
k_D	Water-SPM partition coefficient for inorganic mercury	$l\ Kg^{-1}$	$10^{5.025}$	Melaku Canu et al. (2015)
k_{Ph-de}	Rate constant for the photo-demethylation of methyl-mercury	h^{-1}	0.00216	Monperrus et al. (2007)
k_{me}	Rate constant for the methylation of inorganic mercury	h^{-1}	0.00126	Batrakova et al. (2014)
NPP	Net primary production (yearly average)	$g\ \ C\ m^{-2}\ h^{-1}$	0.020417	D'Ortenzio (2003)
Chl_{surf}	Surface chlorophyll concentrations	$mg\ m^{-3}$	0.205	Sprovieri et al. (2015)
H	Henry's law constant	dimensionless	0.479	Experimental data
u_{wind}	Annual average wind speed	$m\ s^{-1}$	3.83	NASA website
PM_{CO_2}	Molar mass of carbon dioxide	$g\ mol^{-1}$	44.01	Periodic table of the elements
PM_{Hg^0}	Molar mass of elemental mercury	$g\ mol^{-1}$	200.59	Periodic table of the elements
PM_{H_2O}	Molar mass of water	$g\ mol^{-1}$	18.02	Periodic table of the elements
λ	Mercury recycling coefficient for picoeukaryotes population	dimensionless	0.52	Valenti et al. (2017)
D_{w-in}	Molecular diffusion coefficient for inorganic mercury	$m^2\ h^{-1}$	$2.534 \cdot 10^{-6}$	Schulz and Zabel (2006)
D_{w-or}	Molecular diffusion coefficient for methyl-mercury	$m^2\ h^{-1}$	$2.534 \cdot 10^{-6}$	Schulz and Zabel (2006)
δ_{sed}^{II}	Boundary layer thickness above sediment for inorganic mercury	m	0.00009	Ciffroy (2015)
δ_{sed}^{MM}	Boundary layer thickness above sediment for methyl-mercury	m	0.00030	Ciffroy (2015)
δ_w	Boundary layer thickness below sediment	m	0.0001	Sørensen et al. (2001)
K_{demeth}	Rate constant for the de-methylation of methyl-mercury in the pore water of the sediment	h^{-1}	0.007177	Hines et al. (2012)
K_{meth}	Rate constant for the methylation of inorganic mercury in the pore water of the sediment	h^{-1}	0.000503	Hines et al. (2012)
k_{MeHg}	Average fraction of methyl-mercury in the sediment	dimensionless	0.004	Experimental data
K_d^{II}	Sediment - pore water distribution coefficient for inorganic mercury	$l\ Kg^{-1}$	$10^{5.00}$	Liu et al. (2012)
K_d^{MM}	Sediment - pore water distribution coefficient for methyl-mercury	$l\ Kg^{-1}$	$10^{2.50}$	Liu et al. (2012)
α	De-adsorption rate for the total mercury concentration in the sediment	h^{-1}	$1.0 \cdot 10^{-7}$	No data
Hg_D^{bou}	Dissolved mercury concentration at the domain boundaries (Ionian sea)	$ng\ l^{-1}$	0.26	Horvat et al. (2003)
Hg_T^{bou}	Total mercury concentration at the domain boundaries (Ionian sea)	$ng\ l^{-1}$	0.31	Horvat et al. (2003)
L_{Lev}	Levante inlet width	m	400.0	Salvagio Manta et al. (2016)
L_{Sci}	Scirocco inlet width	m	300.0	Salvagio Manta et al. (2016)
$MeHg_{atm}$	Methyl-mercury concentration in atmosphere	$ng\ m^{-3}$	0.0	Driscoll et al. (2013)
Q_{source}	Average flow rate of water for point source	$m^3\ h^{-1}$	0.0	No data
Hg_{source}^0	Elemental mercury concentration of point source	$ng\ l^{-1}$	0.0	No data
Hg_{source}^{II}	Inorganic mercury concentration of point source	$ng\ l^{-1}$	0.0	No data
$MeHg_{source}$	Methyl-mercury concentration of point source	$ng\ l^{-1}$	0.0	No data
S_L^{II}	Direct loads of inorganic mercury	$ng\ l^{-1}\ h^{-1}$	0.0	No data
S_L^{MM}	Direct loads of methyl-mercury	$ng\ l^{-1}\ h^{-1}$	0.0	No data

Table S1: Environmental parameters used in the bio-geochemical model.

Symbol	Interpretation	Unit	Range	Reference
v_x	Horizontal velocity along x-axis (as a function of latitude, longitude, depth and time)	m h^{-1}	$0.0 - 0.5$	Umgiesser (2009)
v_y	Horizontal velocity along y-axis (as a function of latitude, longitude, depth and time)	m h^{-1}	$0.0 - 0.5$	Umgiesser (2009)
f_{org}	Organic fraction of suspended particulate matter in dissolved-phase	dimensionless	$0.004 - 0.010$	Experimental data
k_1	Rate constant for the photo-oxidation of elemental mercury (as a function of time)	h^{-1}	$1.79 - 7.23$	Zhang et al. (2014)
k_2	Rate constant for the photo-reduction of inorganic mercury (as a function of time)	h^{-1}	$0.43 - 1.75$	Zhang et al. (2014)
k_3	Rate constant for the biological oxidation of elemental mercury (as a function of time)	h^{-1}	$0.00252 - 0.00288$	Zhang et al. (2014)
k_4	Rate constant for the biological reduction of inorganic mercury (as a function of time)	h^{-1}	$0.00155 - 0.00177$	Zhang et al. (2014)
$pe - ratio$	Ratio of particulate organic carbon export to NPP out of euphotic zone (as a function of time)	dimensionless	$0.09 - 0.21$	Zhang et al. (2014)
$Hg_{gas-atm}$	Gaseous mercury concentration in atmosphere (as a function of time)	ng m^{-3}	$1.50 - 2.10$	Bagnato et al. (2013)
Hg^{II}_{atm}	Inorganic mercury concentration in atmosphere (as a function of time)	ng l^{-1}	$21.0 - 32.0$	Bagnato et al. (2013)
Pr	Daily amount of precipitation (as a function of time)	mm	$0.41 - 3.33$	NASA website
φ_{sed}	Porosity of the sediment (as a function of latitude, longitude and depth)	dimensionless	$0.000 - 1.000$	Experimental data
TOC_{sed}	Total organic carbon at the sediment surface (as a function of latitude and longitude)	percent dry weight	$0.210 - 4.780$	Experimental data
Hg^{sed}_T	Initial total mercury concentration in sediment (as a function of latitude, longitude and depth)	mg Kg^{-1}	$0.005 - 300.000$	Sprovieri et al. (2011)
SW_{sed}	Specific weight in the surface layer of the sediment (as a function of latitude and longitude)	Kg l^{-1}	$1.14 - 1.98$	Sprovieri et al. (2011)
dep	SPM deposition rate at the seawater-sediment interface (as a function of latitude and longitude)	m y^{-1}	$-0.0070 - 0.0035$	Neumeier et al.(2008)
SPM	Suspended particulate matter conc. in seawater (as a function of latitude, longitude and depth)	mg l^{-1}	$18.4 - 31.0$	Experimental data
R_{in}	Nutrient concentration at the domain boundaries (as a function of depth)	mmol phos. m^{-3}	$0.010 - 0.100$	Experimental data
I_{in}	Incident light intensity at the water surface (as a function of time)	$\mu mol\ ph.$ m^{-2} s^{-1}	$301.37 - 1524.30$	NASA website
$chla_{cell}$	Chl-a cellular content of picoeukaryotes (as a function of depth)	fg chl-a $cell^{-1}$	$10.00 - 660.00$	Brunet et al. (2007)
z_b	Depth of the water column (as a function of latitude and longitude)	m	$0 - 30$	Sprovieri et al. (2015)

Table S2: Environmental variables used in the bio-geochemical model.

Symbol	Interpretation	Unit	Value	Reference
V_{cell}	Picoeukaryotes cell volume	μm^3 cell^{-1}	4188.787	Experimental data
W_{phy}	Picoeukaryotes cell weight	μg cell^{-1}	0.004188787	Strickland (1960)
VFC_{II}	Volume concentration factor for inorganic mercury	l Kg^{-1}	27500	Pickhardt and Fischer (2007)
VFC_{MM}	Volume concentration factor for methyl-mercury	l Kg^{-1}	800000	Pickhardt and Fischer (2007)
a_{growth}	Intercept of phytoplankton growth rate	dimensionless	0.22	Ciffroy (2015)
b_{growth}	Slope of phytoplankton growth rate	dimensionless	0.15	Ciffroy (2015)
k	Allometric rate exponent	dimensionless	0.25	Hendricks at al. (2007)
$p_{carbonphy}$	Organic carbon fraction of phytoplankton	dimensionless	0.29	Ciffroy (2015)
ρ_{lipid}	Lipid-layer permeation resistance	d	32.0	Hauck at al. (2011)
ρ_{water}	Water-layer diffusion resistance	d	0.0068	Hauck at al. (2011)
b_{lipid}	Lipid permeation resistance exponent	dimensionless	0.41	Hendricks at al. (2001)
$log_{10}K_d^{II}$	Water-Dissolved Organic Carbon partition coefficient for inorganic mercury	dimensionless	5.4	Allison and Allison (2005)
$log_{10}K_d^{MM}$	Water-Dissolved Organic Carbon partition coefficient for methyl-mercury	dimensionless	5.0	Allison and Allison (2005)
a_{bg}	Background turbidity	m^{-1}	0.060	Valenti et al. (2017)
a_1	Average absorption coefficient of picoeukaryotes	m^2 mg chl-a $^{-1}$	0.012	Hickman et al. (2010)
a_2	Average absorption coefficient of phytoplankton $> 3\mu m$	m^2 mg chl-a $^{-1}$	0.020	Hickman et al. (2010)
w	Sinking velocity of picoeukaryotes	m h^{-1}	0.000098	Valenti et al. (2017)
r	Maximum specific growth rate of picoeukaryotes	h^{-1}	0.096	Raven et al. (2005)
m_b	Specific loss rate of picoeukaryotes	h^{-1}	0.010	Veldhuis et al. (2005)
K_I	Half-saturation constant of light-limited growth of picoeukaryotes	μmol photons m^{-2} s^{-1}	67.50	Valenti et al. (2017)
K_R	Half-saturation constant of nutrient-limited growth of picoeukaryotes	mmol phosphorus m^{-3}	0.200	Valenti et al. (2017)
$1/Y$	Nutrient content of picoeukaryotes	mmol phosphorus cell^{-1}	2.00×10^{-12}	Timmermans et al. (2005)
ε	Nutrient recycling coefficient of picoeukaryotes	dimensionless	0.52	Valenti et al. (2017)

Table S3: Biological parameters used in the Phytoplankton model for mercury adsorption and Nutrient-Phytoplankton model.

		Experimental data				*Theoretical results*			
Station	*Period*	*Latitude*	*Longitude*	*Depth* $[m]$	$MeHg$ $[ng/l]$	*Latitude*	*Longitude*	*Depth* $[m]$	$MeHg$ $[ng/l]$
$A3$	$19-23/10/17$	37.22650	15.20633	2.00	0.006	37.22708	15.20492	2.50	0.015
$A3$	$19-23/10/17$	37.22650	15.20633	17.00	0.017	37.22708	15.20492	12.50	0.019
$A7$	$19-23/10/17$	37.20467	15.19467	2.00	0.016	37.20638	15.19470	2.50	0.015
$A7$	$19-23/10/17$	37.20467	15.19467	21.00	0.009	37.20638	15.19470	17.50	0.007
$A9$	$19-23/10/17$	37.19333	15.20233	2.00	0.017	37.19396	15.19981	2.50	0.062
$A9$	$19-23/10/17$	37.19333	15.20233	22.00	0.026	37.19396	15.19981	17.50	0.211
$A11$	$19-23/10/17$	37.18333	15.21350	2.00	0.009	37.18155	15.21514	2.50	0.017
$A11$	$19-23/10/17$	37.18333	15.21350	21.00	0.016	37.18155	15.21514	12.50	0.206

Table S4: Methyl-mercury concentration in seawater: comparison between experimental data and theoretical results for all sampling sites investigated during the oceanographic survey of October 2017.

		Experimental data				*Theoretical results*			
Station	*Period*	*Latitude*	*Longitude*	*Depth* $[m]$	Hg_D $[ng/l]$	*Latitude*	*Longitude*	*Depth* $[m]$	Hg_D $[ng/l]$
1	$23-26/05/11$	37.23987	15.20895	1.40	3.200	37.23949	15.21003	2.50	3.081
1	$23-26/05/11$	37.23987	15.20895	6.20	6.700	37.23949	15.21003	7.50	3.729
1	$23-26/05/11$	37.23987	15.20895	11.20	$\leq d.l.$	37.23949	15.21003	12.50	4.812
2	$23-26/05/11$	37.23107	15.20865	2.21	$\leq d.l.$	37.23121	15.21003	2.50	2.665
2	$23-26/05/11$	37.23107	15.20865	6.71	$\leq d.l.$	37.23121	15.21003	7.50	3.079
2	$23-26/05/11$	37.23107	15.20865	10.65	$\leq d.l.$	37.23121	15.21003	12.50	4.174
3	$23-26/05/11$	37.23105	15.19742	2.26	$\leq d.l.$	37.23121	15.19981	2.50	2.591
3	$23-26/05/11$	37.23105	15.19742	4.60	$\leq d.l.$	37.23121	15.19981	2.50	2.591
3	$23-26/05/11$	37.23105	15.19742	8.40	$\leq d.l.$	37.23121	15.19981	7.50	2.918
4	$23-26/05/11$	37.22255	15.19837	0.10	$\leq d.l.$	37.22294	15.19981	2.50	2.603
4	$23-26/05/11$	37.22255	15.19837	3.12	3.200	37.22294	15.19981	7.50	2.603
5	$23-26/05/11$	37.21415	15.20992	1.00	$\leq d.l.$	37.21466	15.21003	2.50	3.101
5	$23-26/05/11$	37.21415	15.20992	9.20	$\leq d.l.$	37.21466	15.21003	7.50	3.494
5	$23-26/05/11$	37.21415	15.20992	15.88	$\leq d.l.$	37.21466	15.21003	12.50	4.086
6	$23-26/05/11$	37.21238	15.21960	1.98	$\leq d.l.$	37.21052	15.22024	2.50	2.346
6	$23-26/05/11$	37.21238	15.21960	6.74	$\leq d.l.$	37.21052	15.22024	7.50	2.375
6	$23-26/05/11$	37.21238	15.21960	13.54	$\leq d.l.$	37.21052	15.22024	12.50	2.139
10	$23-26/05/11$	37.20445	15.19772	1.00	3.200	37.20638	15.19981	2.50	7.139
10	$23-26/05/11$	37.20445	15.19772	9.50	14.300	37.20638	15.19981	7.50	8.256
10	$23-26/05/11$	37.20445	15.19772	19.20	7.300	37.20638	15.19981	17.50	10.333
11	$23-26/05/11$	37.20015	15.20268	1.42	$\leq d.l.$	37.20224	15.20492	2.50	5.090
11	$23-26/05/11$	37.20015	15.20268	10.00	$\leq d.l.$	37.20224	15.20492	7.50	6.067
11	$23-26/05/11$	37.20015	15.20268	18.15	3.300	37.20224	15.20492	17.50	9.084
12	$23-26/05/11$	37.19935	15.21425	1.63	3.200	37.19810	15.21514	2.50	2.824
12	$23-26/05/11$	37.19935	15.21425	13.50	3.200	37.19810	15.21514	12.50	3.794
12	$23-26/05/11$	37.19935	15.21425	23.41	11.800	37.19810	15.21514	22.50	6.532
13	$23-26/05/11$	37.19905	15.22560	2.40	3.200	37.19810	15.22535	2.50	1.335
13	$23-26/05/11$	37.19905	15.22560	16.90	8.900	37.19810	15.22535	17.50	1.698
13	$23-26/05/11$	37.19905	15.22560	29.30	$\leq d.l.$	37.19810	15.22535	27.50	1.629
17	$23-26/05/11$	37.19493	15.20853	1.20	7.500	37.19396	15.21003	2.50	2.514
17	$23-26/05/11$	37.19493	15.20853	11.45	19.800	37.19396	15.21003	12.50	3.701
17	$23-26/05/11$	37.19493	15.20853	21.90	$\leq d.l.$	37.19396	15.21003	22.50	5.573
20	$23-26/05/11$	37.18938	15.20723	0.50	12.600	37.18983	15.20492	2.50	5.949
20	$23-26/05/11$	37.18938	15.20723	11.30	14.600	37.18983	15.20492	12.50	10.531
20	$23-26/05/11$	37.18938	15.20723	16.45	14.600	37.18983	15.20492	17.50	12.035
23	$23-26/05/11$	37.19075	15.21442	2.40	21.300	37.18983	15.21514	2.50	1.890
23	$23-26/05/11$	37.19075	15.21442	11.24	$\leq d.l.$	37.18983	15.21514	12.50	2.834
23	$23-26/05/11$	37.19075	15.21442	20.55	20.300	37.18983	15.21514	22.50	6.050
24	$23-26/05/11$	37.19057	15.22560	1.00	6.000	37.18983	15.22535	2.50	0.842
24	$23-26/05/11$	37.19057	15.22560	9.40	8.900	37.18983	15.22535	7.50	1.050
24	$23-26/05/11$	37.19057	15.22560	16.30	$\leq d.l.$	37.18983	15.22535	17.50	2.102
25	$23-26/05/11$	37.18117	15.21388	1.60	6.000	37.18155	15.21514	2.50	15.360
25	$23-26/05/11$	37.18117	15.21388	7.30	14.600	37.18155	15.21514	7.50	20.939
25	$23-26/05/11$	37.18117	15.21388	12.70	3.200	37.18155	15.21514	12.50	31.524
26	02/02/12	37.17183	15.21913	2.00	$\leq d.l.$	37.17327	15.22024	2.50	1.335
26	02/02/12	37.17183	15.21913	8.00	5.550	37.17327	15.22024	7.50	3.699
27	02/02/12	37.19678	15.23880	2.00	$\leq d.l.$	37.19810	15.23046	2.50	0.208
27	02/02/12	37.19678	15.23880	11.50	$\leq d.l.$	37.19810	15.23046	12.50	1.833
27	02/02/12	37.19678	15.23880	27.00	3.550	37.19810	15.23046	22.50	1.763
7	$23-26/06/12$	37.20963	15.20972	1.00	$\leq d.l.$	37.21052	15.21003	2.50	4.407
7	$23-26/06/12$	37.20963	15.20972	13.50	$\leq d.l.$	37.21052	15.21003	12.50	5.428
7	$23-26/06/12$	37.20963	15.20972	21.00	$\leq d.l.$	37.21052	15.21003	17.50	6.272
15	$23-26/06/12$	37.19495	15.21528	1.00	2.550	37.193964	15.21514	2.50	1.628
15	$23-26/06/12$	37.19495	15.21528	11.50	4.950	37.193964	15.21514	12.50	1.828
15	$23-26/06/12$	37.19495	15.21528	26.00	2.350	37.193964	15.21514	22.50	4.700
21	$23-26/06/12$	37.18813	15.20765	1.00	$\leq d.l.$	37.18983	15.21003	2.50	3.185
21	$23-26/06/12$	37.18813	15.20765	16.00	6.350	37.18983	15.21003	17.50	4.891
21	$23-26/06/12$	37.18813	15.20765	22.00	$\leq d.l.$	37.18983	15.21003	22.50	7.013
*A*3	$19-23/10/17$	37.22650	15.20633	2.00	$\leq d.l.$	37.22708	15.20492	2.50	0.493
*A*3	$19-23/10/17$	37.22650	15.20633	17.00	$\leq d.l.$	37.22708	15.20492	12.50	0.639
*A*7	$19-23/10/17$	37.20467	15.19467	2.00	$\leq d.l.$	37.20638	15.19470	2.50	0.510
*A*7	$19-23/10/17$	37.20467	15.19467	21.00	$\leq d.l.$	37.20638	15.19470	17.50	0.262
*A*9	$19-23/10/17$	37.19333	15.20233	2.00	9.032	37.19396	15.19981	2.50	2.165
*A*9	$19-23/10/17$	37.19333	15.20233	22.00	17.785	37.19396	15.19981	17.50	7.157
*A*11	$19-23/10/17$	37.18333	15.21350	2.00	$\leq d.l.$	37.18155	15.21514	2.50	0.568
*A*11	$19-23/10/17$	37.18333	15.21350	21.00	6.545	37.18155	15.21514	12.50	6.892

Table S5: Dissolved mercury concentration: comparison between experimental data and theoretical results for all sampling sites. The detection limit (d.l.) for mercury concentration is set at 1.9 ng/l.

		Experimental data				*Theoretical results*			
Station	*Period*	*Latitude*	*Longitude*	*Depth* $[m]$	Hg_T $[ng/l]$	*Latitude*	*Longitude*	*Depth* $[m]$	Hg_T $[ng/l]$
1	23 − 26/05/11	37.23987	15.20895	1.40	9.171	37.23949	15.21003	2.50	9.036
1	23 − 26/05/11	37.23987	15.20895	6.20	9.171	37.23949	15.21003	7.50	10.642
1	23 − 26/05/11	37.23987	15.20895	11.20	17.771	37.23949	15.21003	12.50	13.362
2	23 − 26/05/11	37.23107	15.20865	2.21	$\leq d.l.$	37.23121	15.21003	2.50	7.963
2	23 − 26/05/11	37.23107	15.20865	6.71	14.871	37.23121	15.21003	7.50	8.851
2	23 − 26/05/11	37.23107	15.20865	10.65	17.671	37.23121	15.21003	12.50	11.538
3	23 − 26/05/11	37.23105	15.19742	2.26	$\leq d.l.$	37.23121	15.19981	2.50	7.722
3	23 − 26/05/11	37.23105	15.19742	4.60	11.971	37.23121	15.19981	2.50	7.722
3	23 − 26/05/11	37.23105	15.19742	8.40	29.971	37.23121	15.19981	7.50	8.389
4	23 − 26/05/11	37.22255	15.19837	0.10	$\leq d.l.$	37.22294	15.19981	2.50	7.764
4	23 − 26/05/11	37.22255	15.19837	3.12	6.271	37.22294	15.19981	7.50	7.764
5	23 − 26/05/11	37.21415	15.20992	1.00	9.171	37.21466	15.21003	2.50	9.268
5	23 − 26/05/11	37.21415	15.20992	9.20	7.071	37.21466	15.21003	7.50	10.053
5	23 − 26/05/11	37.21415	15.20992	15.88	17.671	37.21466	15.21003	12.50	11.309
6	23 − 26/05/11	37.21238	15.21960	1.98	6.271	37.21052	15.22024	2.50	6.648
6	23 − 26/05/11	37.21238	15.21960	6.74	3.371	37.21052	15.22024	7.50	6.739
6	23 − 26/05/11	37.21238	15.21960	13.54	20.571	37.21052	15.22024	12.50	6.083
10	23 − 26/05/11	37.20445	15.19772	1.00	4.271	37.20638	15.19981	2.50	22.032
10	23 − 26/05/11	37.20445	15.19772	9.50	15.871	37.20638	15.19981	7.50	24.752
10	23 − 26/05/11	37.20445	15.19772	19.20	14.871	37.20638	15.19981	17.50	29.204
11	23 − 26/05/11	37.20015	15.20268	1.42	14.871	37.20224	15.20492	2.50	14.692
11	23 − 26/05/11	37.20015	15.20268	10.00	14.871	37.20224	15.20492	7.50	17.860
11	23 − 26/05/11	37.20015	15.20268	18.15	23.471	37.20224	15.20492	17.50	27.887
12	23 − 26/05/11	37.19935	15.21425	1.63	17.671	37.19810	15.21514	2.50	7.755
12	23 − 26/05/11	37.19935	15.21425	13.50	3.371	37.19810	15.21514	12.50	11.131
12	23 − 26/05/11	37.19935	15.21425	23.41	19.271	37.19810	15.21514	22.50	19.998
13	23 − 26/05/11	37.19905	15.22560	2.40	17.671	37.19810	15.22535	2.50	3.634
13	23 − 26/05/11	37.19905	15.22560	16.90	12.671	37.19810	15.22535	17.50	4.876
13	23 − 26/05/11	37.19905	15.22560	29.30	3.371	37.19810	15.22535	27.50	4.703
17	23 − 26/05/11	37.19493	15.20853	1.20	26.271	37.19396	15.21003	2.50	6.806
17	23 − 26/05/11	37.19493	15.20853	11.45	129.271	37.19396	15.21003	12.50	11.364
17	23 − 26/05/11	37.19493	15.20853	21.90	127.071	37.19396	15.21003	22.50	18.212
20	23 − 26/05/11	37.18938	15.20723	0.50	12.600	37.18983	15.20492	2.50	15.983
20	23 − 26/05/11	37.18938	15.20723	11.30	23.500	37.18983	15.20492	12.50	33.232
20	23 − 26/05/11	37.18938	15.20723	16.45	28.200	37.18983	15.20492	17.50	40.937
23	23 − 26/05/11	37.19075	15.21442	2.40	23.371	37.18983	15.21514	2.50	5.060
23	23 − 26/05/11	37.19075	15.21442	11.24	20.571	37.18983	15.21514	12.50	7.835
23	23 − 26/05/11	37.19075	15.21442	20.55	57.771	37.18983	15.21514	22.50	17.255
24	23 − 26/05/11	37.19057	15.22560	1.00	11.971	37.18983	15.22535	2.50	2.253
24	23 − 26/05/11	37.19057	15.22560	9.40	18.671	37.18983	15.22535	7.50	2.839
24	23 − 26/05/11	37.19057	15.22560	16.30	2.271	37.18983	15.22535	17.50	5.873
25	23 − 26/05/11	37.18117	15.21388	1.60	22.571	37.18155	15.21514	2.50	40.701
25	23 − 26/05/11	37.18117	15.21388	7.30	31.971	37.18155	15.21514	7.50	54.959
25	23 − 26/05/11	37.18117	15.21388	12.70	34.871	37.18155	15.21514	12.50	82.142
26	02/02/12	37.17183	15.21913	2.00	4.554	37.17327	15.22024	2.50	3.487
26	02/02/12	37.17183	15.21913	8.00	11.054	37.17327	15.22024	7.50	9.696
27	02/02/12	37.19678	15.23880	2.00	4.554	37.19810	15.23046	2.50	0.563
27	02/02/12	37.19678	15.23880	11.50	4.804	37.19810	15.23046	12.50	5.187
27	02/02/12	37.19678	15.23880	27.00	6.104	37.19810	15.23046	22.50	5.017
7	23 − 26/06/12	37.20963	15.20972	1.00	1.854	37.21052	15.21003	2.50	12.814
7	23 − 26/06/12	37.20963	15.20972	13.50	9.854	37.21052	15.21003	12.50	15.627
7	23 − 26/06/12	37.20963	15.20972	21.00	1.750	37.21052	15.21003	17.50	18.185
15	23 − 26/06/12	37.19495	15.21528	1.00	5.954	37.193964	15.21514	2.50	4.411
15	23 − 26/06/12	37.19495	15.21528	11.50	8.554	37.193964	15.21514	12.50	5.292
15	23 − 26/06/12	37.19495	15.21528	26.00	15.687	37.193964	15.21514	22.50	14.263
21	23 − 26/06/12	37.18813	15.20765	1.00	1.020	37.18983	15.21003	2.50	8.552
21	23 − 26/06/12	37.18813	15.20765	16.00	14.854	37.18983	15.21003	17.50	14.235
21	23 − 26/06/12	37.18813	15.20765	22.00	18.090	37.18983	15.21003	22.50	21.356
*A*3	19 − 23/10/17	37.22650	15.20633	2.00	$\leq d.l.$	37.22708	15.20492	2.50	1.483
*A*3	19 − 23/10/17	37.22650	15.20633	17.00	$\leq d.l.$	37.22708	15.20492	12.50	1.764
*A*7	19 − 23/10/17	37.20467	15.19467	2.00	$\leq d.l.$	37.20638	15.19470	2.50	1.597
*A*7	19 − 23/10/17	37.20467	15.19467	21.00	$\leq d.l.$	37.20638	15.19470	17.50	0.747
*A*9	19 − 23/10/17	37.19333	15.20233	2.00	12.182	37.19396	15.19981	2.50	5.811
*A*9	19 − 23/10/17	37.19333	15.20233	22.00	25.132	37.19396	15.19981	17.50	26.517
*A*11	19 − 23/10/17	37.18333	15.21350	2.00	$\leq d.l.$	37.18155	15.21514	2.50	1.505
*A*11	19 − 23/10/17	37.18333	15.21350	21.00	12.482	37.18155	15.21514	12.50	18.270

Table S6: Total mercury concentration: comparison between experimental data and theoretical results for all sampling sites. The detection limit (d.l.) for mercury concentration is set at 1.9 ng/l.

		Experimental data			*Theoretical results*		
Station	*Period*	*Latitude*	*Longitude*	*Benthic flux* [$\mu g/(\mathrm{m}^2\ \mathrm{d})$]	*Latitude*	*Longitude*	*Benthic flux* [$\mu g/(\mathrm{m}^2\ \mathrm{d})$]
9	$19-21/09/11$	37.20615	15.20497	23.000	37.20638	15.20492	35.926
18	$19-21/09/11$	37.18823	15.20403	56.000	37.18983	15.20492	46.647
22	$19-21/09/11$	37.19010	15.20953	8.700	37.18983	15.21003	22.860
7	$23-26/06/12$	37.20963	15.20972	23.000	37.21052	15.21003	20.177
15	$23-26/06/12$	37.19495	15.21528	92.000	37.19396	15.21514	102.147
21	$23-26/06/12$	37.18813	15.20765	21.000	37.18983	15.21003	21.373

Table S7: Benthic mercury flux: comparison between experimental data and theoretical results for six sampling sites.

		Experimental data			*Theoretical results*		
Station	*Period*	*Latitude*	*Longitude*	*Atmospheric flux* $[ng/(\mathrm{m}^2\ \mathrm{h})]$	*Latitude*	*Longitude*	*Atmospheric flux* $[ng/(\mathrm{m}^2\ \mathrm{h})]$
$ST1$	29/11/11	37.19352	15.21455	36.000	37.19396	15.21514	34.426
$ST2$	29/11/11	37.21569	15.19763	14.400	37.21466	15.19981	15.039
$ST3$	30/11/11	37.17957	15.20695	72.000	37.18155	15.20492	57.571
$ST5$	24/06/12	37.20951	15.20962	10.800	37.21052	15.21003	23.054
$ST6$	23/06/12	37.19470	15.21552	7.200	37.19396	15.21514	8.440
$ST7$	25/06/12	37.18814	15.20757	18.000	37.18983	15.21003	16.623

Table S8: Mercury evasion flux: comparison between experimental data and theoretical results for six sampling sites.

Symbol	Interpretation	Year	Unit	Value
O_{Lev_1}	Total mercury outflow from the Levante inlet to the open sea	2005	$Kmol/year$	0.071
O_{Sci_1}	Total mercury outflow from the Scirocco inlet to the open sea	2005	$Kmol/year$	0.195
O_1	Total mercury outflow from the basin to the open sea	2005	$Kmol/year$	0.265
$R_{Hg^{II}{}_1}$	Inorganic mercury release from the sediment of the basin	2005	$Kmol/year$	3.024
R_{MeHg_1}	Methyl-mercury release from the sediment of the basin	2005	$Kmol/year$	0.096
R_1	Dissolved mercury release from the sediment of the basin	2005	$Kmol/year$	3.120
V_1	Gaseous elemental mercury evasion from the basin into the atmosphere	2005	$Kmol/year$	0.021
S_1	Amount of mercury recycled for scavenging within the Augusta basin	2005	$Kmol/year$	0.376
D_1	Total mercury recycled within the Augusta basin	2005	$Kmol/year$	2.835
O_{Lev_2}	Total mercury outflow from the Levante inlet to the open sea	2011	$Kmol/year$	0.059
O_{Sci_2}	Total mercury outflow from the Scirocco inlet to the open sea	2011	$Kmol/year$	0.132
O_2	Total mercury outflow from the basin to the open sea	2011	$Kmol/year$	0.191
$R_{Hg^{II}{}_2}$	Inorganic mercury release from the sediment of the basin	2011	$Kmol/year$	2.584
R_{MeHg_2}	Methyl-mercury release from the sediment of the basin	2011	$Kmol/year$	0.073
R_2	Dissolved mercury release from the sediment of the basin	2011	$Kmol/year$	2.657
V_2	Gaseous elemental mercury evasion from the basin into the atmosphere	2011	$Kmol/year$	0.018
S_2	Amount of mercury recycled for scavenging within the Augusta basin	2011	$Kmol/year$	0.322
D_2	Total mercury recycled within the Augusta basin	2011	$Kmol/year$	2.450
O_{Lev_3}	Total mercury outflow from the Levante inlet to the open sea	2017	$Kmol/year$	0.052
O_{Sci_3}	Total mercury outflow from the Scirocco inlet to the open sea	2017	$Kmol/year$	0.111
O_3	Total mercury outflow from the basin to the open sea	2017	$Kmol/year$	0.164
$R_{Hg^{II}{}_3}$	Inorganic mercury release from the sediment of the basin	2017	$Kmol/year$	2.390
R_{MeHg_3}	Methyl-mercury release from the sediment of the basin	2017	$Kmol/year$	0.067
R_3	Dissolved mercury release from the sediment of the basin	2017	$Kmol/year$	2.458
V_3	Gaseous elemental mercury evasion from the basin into the atmosphere	2017	$Kmol/year$	0.016
S_3	Amount of mercury recycled for scavenging within the Augusta basin	2017	$Kmol/year$	0.295
D_3	Total mercury recycled within the Augusta basin	2017	$Kmol/year$	2.279
O_{Lev_4}	Total mercury outflow from the Levante inlet to the open sea	2054	$Kmol/year$	0.038
O_{Sci_4}	Total mercury outflow from the Scirocco inlet to the open sea	2054	$Kmol/year$	0.078
O_4	Total mercury outflow from the basin to the open sea	2054	$Kmol/year$	0.117
$R_{Hg^{II}{}_4}$	Inorganic mercury release from the sediment of the basin	2054	$Kmol/year$	1.929
R_{MeHg_4}	Methyl-mercury release from the sediment of the basin	2054	$Kmol/year$	0.054
R_4	Dissolved mercury release from the sediment of the basin	2054	$Kmol/year$	1.983
V_4	Gaseous elemental mercury evasion from the basin into the atmosphere	2054	$Kmol/year$	0.013
S_4	Amount of mercury recycled for scavenging within the Augusta basin	2054	$Kmol/year$	0.230
D_4	Total mercury recycled within the Augusta basin	2054	$Kmol/year$	1.855
O_{Lev_5}	Total mercury outflow from the Levante inlet to the open sea	2104	$Kmol/year$	0.032
O_{Sci_5}	Total mercury outflow from the Scirocco inlet to the open sea	2104	$Kmol/year$	0.067
O_5	Total mercury outflow from the basin to the open sea	2104	$Kmol/year$	0.099
$R_{Hg^{II}{}_5}$	Inorganic mercury release from the sediment of the basin	2104	$Kmol/year$	1.699
R_{MeHg_5}	Methyl-mercury release from the sediment of the basin	2104	$Kmol/year$	0.048
R_5	Dissolved mercury release from the sediment of the basin	2104	$Kmol/year$	1.746
V_5	Gaseous elemental mercury evasion from the basin into the atmosphere	2104	$Kmol/year$	0.011
S_5	Amount of mercury recycled for scavenging within the Augusta basin	2104	$Kmol/year$	0.198
D_5	Total mercury recycled within the Augusta basin	2104	$Kmol/year$	1.638
O_{Lev_6}	Total mercury outflow from the Levante inlet to the open sea	2254	$Kmol/year$	0.022
O_{Sci_6}	Total mercury outflow from the Scirocco inlet to the open sea	2254	$Kmol/year$	0.054
O_6	Total mercury outflow from the basin to the open sea	2254	$Kmol/year$	0.076
$R_{Hg^{II}{}_6}$	Inorganic mercury release from the sediment of the basin	2254	$Kmol/year$	1.351
R_{MeHg_6}	Methyl-mercury release from the sediment of the basin	2254	$Kmol/year$	0.038
R_6	Dissolved mercury release from the sediment of the basin	2254	$Kmol/year$	1.389
V_6	Gaseous elemental mercury evasion from the basin into the atmosphere	2254	$Kmol/year$	0.009
S_6	Amount of mercury recycled for scavenging within the Augusta basin	2254	$Kmol/year$	0.151
D_6	Total mercury recycled within the Augusta basin	2254	$Kmol/year$	1.306
A	Input of dissolved mercury from anthropogenic activities		$Kmol/year$	0.000
AD	Atmospheric mercury deposition		$Kmol/year$	$1.733 \cdot 10^{-3}$

Table S9: Mass balance of mercury in the Augusta basin simulated for six different years (2005, 2011, 2017, 2054, 2104, and 2254).

		Experimental data				*Theoretical results*			
Station	*Period*	*Latitude*	*Longitude*	*Depth* $[m]$	Hg_{pw} $[ng/l]$	*Latitude*	*Longitude*	*Depth* $[m]$	Hg_{pw} $[ng/l]$
8	$23-26/05/11$	37.21030	15.20788	0.11	87.225	37.21052	15.21003	0.10	90.129
16	$23-26/05/11$	37.19697	15.20900	0.11	98.538	37.19810	15.21003	0.10	94.235

Table S10: Mercury concentration in the pore water: comparison between experimental data and theoretical results for the sampling sites investigated during the oceanographic survey of May 2011.